Lysozyme-encapsulated gold nanoclusters as a potential therapy for Alzheimer's disease

A Thesis submitted to the University of Strathclyde for the degree of Master of Philosophy

by

Carla McVay

Strathclyde Institute of Pharmacy and Biomedical Sciences
University of Strathclyde
Glasgow

2025

Contents

Abstract

Background: Alzheimer's disease (AD), the most common cause of dementia, is characterised by synaptic loss and neurodegeneration. Amyloid-β (Aβ) accumulation into plaques, hyperphosphorylation of tau protein, and neurofibrillary tangles (NFTs) in the brain are considered the pathological hallmarks of AD. However, more recent evidence suggests that neuroinflammation plays a key role in the pathophysiology of AD and causes dysregulated cellular activity and neurodegeneration by over-activating microglia. Novel lysozyme-encapsulated gold nanoclusters have immunomodulatory roles like inhibiting the formation Aβ plaques via the modulation of immune responses mediated by microglial cells and can therefore be used as a new therapy for AD.

Hypothesis: Lysozyme-encapsulated gold nanoclusters (Lys-AuNCs) influence AD pathology through modulating immune responses mediated by microglial cells and hence may be used as a therapy for AD.

Methodology: Lys-AuNCs were synthesised using a modified 'one-pot process' adding filtration to account for sterile cell culture. Lys-AuNCs were characterised through fluorescent lifetime measurements with concentrations calculated from calibration curves to ensure physiochemical and optical properties remained intact. Activation of microglial cell line HMC3 by Lys-AuNCs was confirmed by positive staining with microglia marker IBA-1, then microglial phenotype was investigated through cell morphological analysis via phase imaging. Toxicity of Lys-AuNCs on HMC3s was determined via MTT assay. Localisation of Lys-AuNCs were visualised via z-stack imaging of HMC3 cells. Pro- and anti-inflammatory markers iNOS and Arg-1 expression induced by Lys-AuNCs were assessed through staining and quantified using ImageJ software.

Results: HMC3 cells displayed resting morphology when treated with concentrations of Lys-AuNCs ranging from 50-600 μg/mL with some cells displaying activated morphology at 200 μg/mL. Lys-AuNCs induced a slight decrease in viability in HMC3 cells at 600 μg/mL after 72 hours (-88.9%;*p<0.05) compared to untreated cells, with no significant decrease in viability across other concentrations. HMC3 cells treated with 10 μg/mL of Lys-AuNCs showed an increase in iNOS expression with no significant changes seen in other concentrations (5, 50 and 200 μg/mL) (**p<0.01). Treated cells showed a significant reduction

in Arg-1 expression across all concentrations (5, 10, 50 and 200 μg/mL) (****p<0.0001). Cells treated with 50 and 200 μg/mL of Lys-AuNCs showed intracellular localisation of clusters in HMC3 cells with staining and confocal imaging.

Conclusions: Results showed that Lys-AuNCs induced minimal toxicity in HMC3 cells treated with 600 μg/ mL after 72 hours and no toxicity in all other concentrations. It can be confirmed that Lys-AuNCs can activate and modulate the immune response of microglial cells with morphology changes and marked pro-inflammatory mediator expression thus, targeting microglia should be further investigated as it may provide a potential effective therapy against AD.

Abbreviations

AβOs- Aβ oligomers

ACh- acetylcholine

ACID- APP intracellular domain

AD- Alzheimer's disease

ADI- Alzheimer's Disease International

APOE- apolipoprotein E

APP- amyloid precursor protein

Arg-1- arginase 1

ATP- adenosine triphosphate

Au- gold

Aβ- amyloid-beta

BBB- blood brain barrier

BDNF- brain-derived neurotrophic factor

BSA- bovine serum albumin

BSA-AuNCs- bovine serum albumin-encapsulated gold nanoclusters

CBF- cerebrospinal fluid

CD- cluster of differentiation

ChEIs- cholinesterase inhibitors

CNS- central nervous system

CSF- cerebrospinal fluid

CTF- c-terminal fragment

DAM- disease-associated microglia

DAMPs- damage-associated molecular patterns

DAP12- DNAX-activating protein of 12 kDa

DAPI- 4′,6-diamidino-2-phenylindole

ELISA- enzyme linked immunosorbent assay

EOAD- early onset Alzheimer's disease

FDA- Food and Drug Administration

FDG-PET- fluorodeoxyglucose-positron emission tomography

GABA- gamma-aminobutyric acid

GFAP- glial fibrillary acidic protein

HDL- high density lipoprotein

HDL- high-density lipoprotein

HLA- human leukocyte antigen

HLA-DR- Human leukocyte antigen-D related

HSA- human serum albumin

IBA1- ionised calcium-binding adaptor molecule 1

IGF-1- insulin-like growth factor

IL- interleukin

iNOS- inducible nitric oxide

LOAD- late onset Alzheimer's disease

LPS- lipopolysaccharide

Lys- lysozyme

Lys-AuNC- lysozyme-encapsulated gold nanocluster

MAP- microtubule associated protein

MHC- major histocompatibility complex

MTT- 3-(4,5-dimethylthiazol-2-yl)-2,5-diphenyl-2H-tetrazolium bromide

NADPH- nicotinamide adenine dinucleotide phosphate hydrogen

NC- nanocluster

NFT- neurofibrillary tangle

NMDA- N-methyl-D-aspartate

NO- nitric oxide

NOD- nucleotide-binding oligomerisation domains

NOS- nitric oxide species

NOX2- NADPH oxidase 2

NP- nanoparticle

NVU- neurovascular unit

ONS- Office of National Statistics

PGRN- progranulin

PRRs- pattern recognition receptors

PSEN- presenilin

ROS- reactive oxygen species

RT- room temperature

TGF- transforming growth factor

TLR- toll-like receptor

TNF- tumour necrosis factor

TREM2- triggering receptor expressed on myeloid cells 2

1. Introduction

1.1 Introduction to dementia and Alzheimer's disease

Dementia and Alzheimer's Disease (AD) have been the leading causes of death in the UK for the last 8 years according to the Office of National Statistics (ONS) (1). Dementia is a term that describes a pattern of memory decline and accounts for many neuro-related diseases all of which are characterised by progressive cognitive impairment. This state of neurodegeneration results in a decline in function of at least one other domains of cognition such as thinking, personality, language, praxis, attention, judgement, behaviour, social and visuospatial skills (2). Alzheimer's Disease International (ADI) states that roughly 75% of people with dementia remain undiagnosed which could potentially increase to 90% in developing countries (3). AD is the most common progressive form of dementia affecting over 55 million people worldwide with a potential reach of 78 million by 2030 (4). An issue with AD is its social impact and with an aging population, the rapid growth rate of AD cases poses a major economic burden on caregivers and the public-health care sector and can be deemed as a public health crisis. Symptoms can reach a severity to reduce patient's quality of life, losing all language ability and motor function leading to hospitalisation and eventually death.

1.2 Risk factors of AD

1.2.1 Genetic risk factors

The exact cause of AD is not clear, however there are genetic and environmental factors that increase susceptibility to the disease. Early-onset AD (EOAD) also known as familial AD typically occurs between the ages of 35 and 65 constituting roughly 5% of AD patients. EOAD cases can be inherited in an autosomal dominant fashion by a mutation in any one of three genes such as, the amyloid precursor protein (APP) and the presenilin 1 and 2 genes (PSEN1 and PSEN2) (5). Late-onset AD (LOAD) also known as sporadic AD is the most common form of AD that affects over 95% of patients and numerous studies have shown is associated with Ɛ4 allele variant of the apolipoprotein E (APOE) gene increasing the risk of LOAD (6). APOE is a key protein component of high-density lipoprotein (HDL)- like lipoprotein and influences AD through its presence in Aβ plaques and its key role in the clearance and deposition of Aβ (7). It has been seen that APOE4 is the most prominent risk factor for LOAD and APOE polymorphism is a main risk factor for AD progression. A study showed APOE4 mice to have increased glial activation in response to lipopolysaccharides (LPS) compared to APOE2 and

APOE3 transgenic mice further suggesting that APOE polymorphism is modulating AD progression (8). Studies have shown APOE2 to decrease the risk of LOAD through protective mechanisms against AD, such as the reduction of Aβ deposition and neuroprotective roles such as regulation in lipid metabolism and synaptic function (9, 10). Studies have shown AD to have a preclinical stage that can precede the onset of clinical symptoms by up to several years and in this case, when clinical symptoms become apparent, pathology is already well established in the brain and clinical intervention only treats symptoms to slow progression of disease. Early diagnosis of AD is therefore essential to provide opportunities to intervene before irreversible neuropathology takes places (11, 12).

1.2.2 Environmental risk factors

Environmental factors can also contribute to the increased risk of AD such as aging, diet, traumatic brain injury, vascular risk factors and sleep disorders (13, 14, 15). Research shows increasing evidence for a supporting role of diets in AD with dietary factors such as saturated fats, excessive alcohol, and calorie intake to be associated with oxidative stress and neurological damage seen in AD which can also support other AD risk factors such as diabetes and hyperinsulinemia. In contrast diets rich in antioxidants, nutrients and vitamins have said to be protective against the disease, however the relationship between particular diets and cognitive changes needs to be confirmed at a clinical level (16).

1.3 Pathophysiology of AD

AD is a heterogenous disease with pathological hallmarks including the presence of extracellular beta-amyloid (Aβ) deposition as neuritic plaques, the accumulation of intracellular hyperphosphorylated tau as neurofibrillary tangles (NFTs) and gliosis-mediated neuroinflammation. The exact mechanisms to which Aβ protein operates in AD are still unknown, although research can confirm the accumulation of Aβ triggers a loss of connections between synapses and neurons in the brain, resulting in neuronal damage and death. This can result in a significant loss in brain volume known as brain atrophy towards the late stages of disease, especially in the cerebral cortex and hippocampus region. The hippocampus is an area of the brain crucial for memory and is one of the first areas to be affected by significant tissue loss in AD leading to disconnection of other regions of the brain (Fig 1) (17, 18).

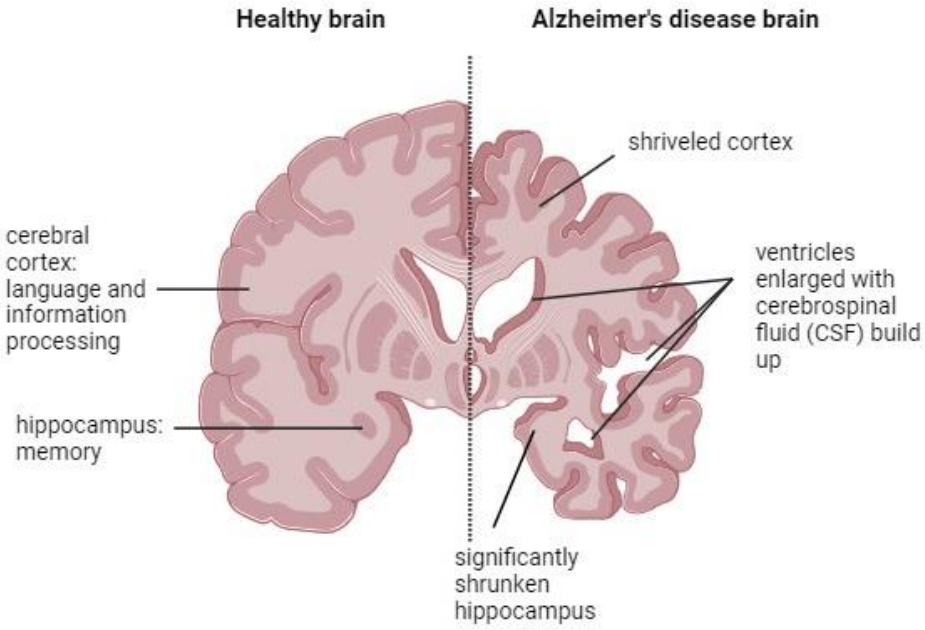

Figure 1. Healthy brain vs Alzheimer's disease brain. Diagram shows the main brain regions and their associated functions affected by atrophy in AD. Significant atrophy can be seen in the hippocampus and cortex as a result of abundant neuronal cell death and damage which presents as clinical manifestations such as reduced language, thinking and memory.

1.3.1 Amyloid beta (Aβ)

The 'amyloid hypothesis' was developed based on the discovery that the over accumulation of fibrillogenic Aβ in the form of senile plaques in the brain is the major event in AD that triggers hyperphosphorylated tau deposition, neuron and synaptic impairment and neuroinflammation (19). The hypothesis depicts the production of pathogenic Aβ peptides from glycoprotein APP into senile plaques via oligomerisation and fibrilisation of Aβ peptides, also known as, the amyloidogenic pathway. These senile plaques accumulate in the AD brain and impair synaptic function and structure leading to neuronal cell death and neurodegeneration (Fig 2) (20, 21). Aβ40 and Aβ42 are two major isoforms of Aβ with Aβ42 exhibiting rapid aggregation forming fibrils in the centre of neuritic plaques in AD. Studies found significant Aβ deposition in the brains of aged APP/PS1 mice with minimal to no Aβ deposition found in age-matched controls (22). These transgenic mouse models are widely used in the study of Aβ pathology and evaluation of anti-amyloid treatments. Aβ plaques are primarily deposited in the medial prefrontal cortex followed by the hippocampus, basal ganglia, thalamus and basal forebrain and in the late stages of disease reaches the brain stem and cerebellum (23, 24). Many studies

involving the biochemical analysis of APP and presenilin genes greatly enhanced the understanding of molecular pathways that lead to Aβ production and hence lead to focus on the development of disease-modifying treatments for AD based on Aβ (25, 26).

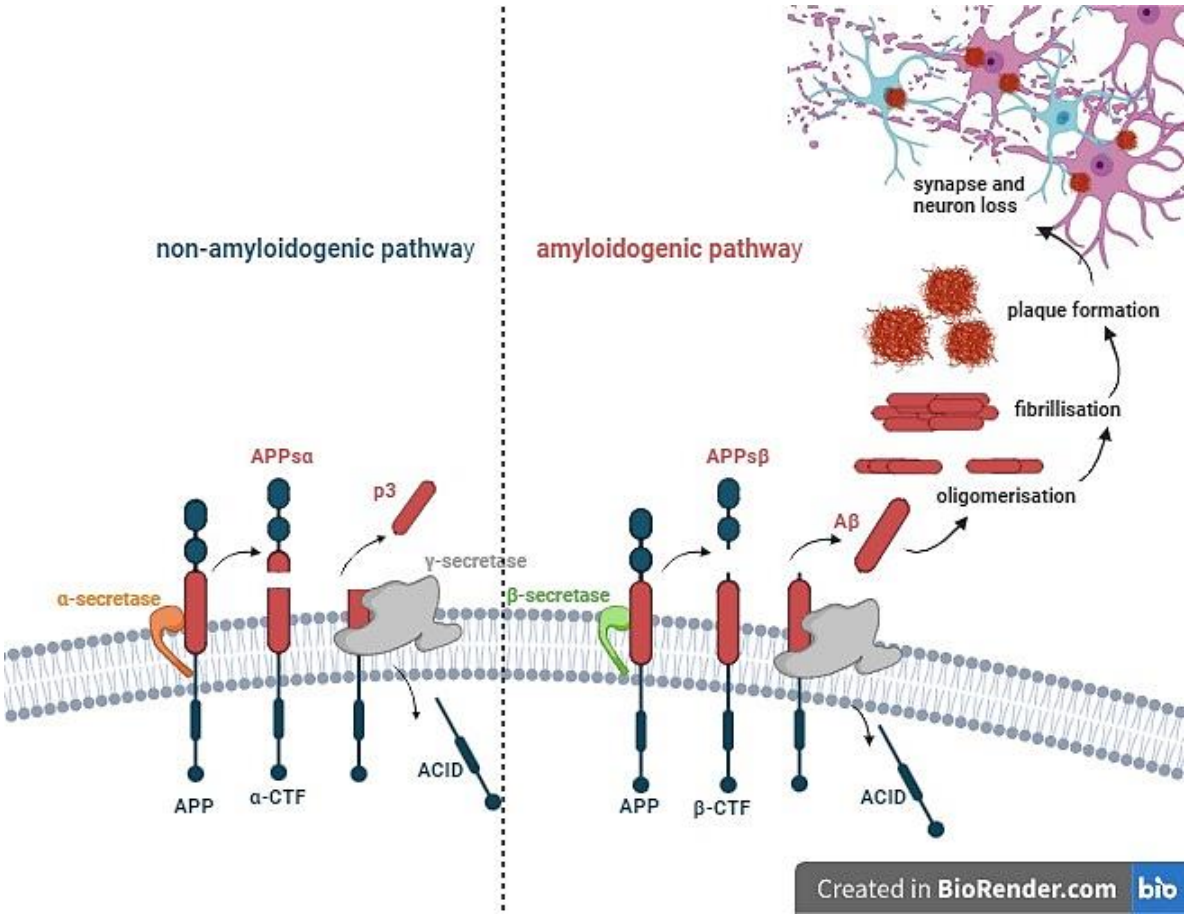

Created with BioRender.com

Figure 2. Amyloidogenic and non-amyloidogenic processing of APP. In normal conditions APP is processed through the **non-amyloidogenic** pathway where APP is cleaved by α-secretase within the Aβ domain. A N-terminal fragment (APPs α) s generated which promotes neuronal survival and a membrane bound C-terminal fragment (α-CTF). α-CTF is cleaved by γ-secretase producing extracellular p3 peptide and an APP intracellular domain (ACID). During **amyloidogenic** processing, Aβ peptide is produced by transmembrane enzymes β-secretase specifically BACE1 and mutated γ-secretase that cleave APP releasing secreted APP-β (APPsβ), leaving the amyloidogenic component bound. Subsequent cleavage of APP by γ-secretase holds the Aβ40/42 isoforms and ACID. γ-secretase continuous to cleave APP at various sites producing Aβ peptides that range in length from 38 to 48 amino acids that start to oligomerise and form fibrils that eventually form neuritic plaques that lead to neurodegeneration in AD.

It could be the prioritised focus on the amyloid cascade hypothesis as a foundation for preclinical research that leads to the continuous failed mid-to-late-stage clinical trials which also fuels the progressive lack of support from corporations for drug development for AD. Neuropathological lesions seen in AD such as Aβ plaques are also present in elderly patients without dementia, and so focus on reducing these particular lesions will not always result in clinical efficacy (27). Several clinical and neuropathological manifestations of AD are apparent with the normal process of aging making distinguishing between symptoms of normal aging and abnormal development with AD difficult. This is why focus should be diverted to advancing understanding on key molecular and cellular mechanisms implicated in AD for novel therapeutic approaches.

1.3.2 Neurofibrillary tangles (NFTs)

Although the amyloid hypothesis remains a dominant hallmark of AD it sparks controversy with research showing that reductions in Aβ pathology don't always correlate to cognitive decline and slow the progression of AD (28, 29). Recent research focuses more on Aβ oligomers (AβOs) as these have shown to elicit neurotoxicity independent to larger fibrils and plaques suggesting AβOs trigger memory dysfunction seen in AD (30). NFTs of phosphorylated tau protein has been shown to correlate to cognitive decline in AD. Under physiological conditions, tau is a microtubule associated protein that regulates the assembly and maintenance of microtubules through phosphorylation providing support and stabilisation to the cytoskeleton of neurons (31, 32). In the AD brain, aberrant hyperphosphorylation of tau causes the breakdown of microtubules and promotes its aggregation into paired helical filaments that eventually form NFTs. These cause synapse loss and neuronal apoptosis which leads to neurodegeneration seen in AD (33, 34). Prior to the formation of NFTs, tau phosphorylation is said to be the key event in the toxic spread of this protein via synapses and research shows varied tauopathy mutations can ready tau to be phosphorylated (35). Studies have shown Aβ deposition and tau pathology to have synergic effects which can be supported by the continuous failed clinical trials for anti-Aβ therapies (36).

1.4 Microglia and neuroinflammation

The CNS consists of neurons and glial cells and some of the main glial cells include microglia, astrocytes and oligodendrocytes. These cells function to maintain neuronal homeostasis in the brain through regulatory mechanisms in cell-to-cell signalling and the maintenance function of

synapses. Homeostatic disruption may accelerate the progression of neurodegenerative diseases such as AD (37). More recent research has focused on glial-mediated neuroinflammation as one of the main features of AD pathology. Studies done *in vivo* and *in vitro* have shown inflammation to cause cognitive impairment, neuronal cell death and synapse loss. As well as high expression of various neuroinflammatory markers reported in the brains of AD patients and animal models of AD. This has led to the neuroinflammatory hypothesis of AD, characterised by the abnormal activation of immune cells of the brain that lead to neuronal damage and death in AD (38). Microglia are known as the resident immune cells of the brain as they are tasked as the first responders to induce an inflammatory response against infection or injury. Inflammation induced by activated microglia is thought to play a neuroprotective role in normal physiological conditions with Aβ activating microglia to bind and remove plaques via phagocytosis. As AD progresses, microglia are over activated and become defective resulting in a chronic inflammatory response (neuroinflammation) in the CNS that exacerbates Aβ pathologies fuelling neurodegeneration in AD. This sustained activation of glial cells such as microglia and astrocytes is known as reactive gliosis induced near sites of Aβ plaques (39, 40, 41).

1.4.1 States of microglia

Extensive research has shown microglia to have key roles in the maintenance of a healthy brain such as synaptic plasticity, neuronal activity and maintaining CNS homeostasis (42). Studies have also shown microglial-induced synapse depletion in aged mice in various regions of the CNS (43). Unlike other glial cells such as astrocytes and oligodendrocytes microglia arise from erythromyeloid precursors formed in the yolk sack where they migrate to the CNS in the early stages of embryonic development. Research has led many people to believe that microglia only possess two different states being ‘resting’ characterised by highly ramified morphology and ‘activated’ characterised by amoeboid shape. This paradigm has contributed to the misconception that microglia in the healthy brain are functionally quiescent in the apparent ‘resting’ state, and the transition to amoeboid during pathologic processes was the key criteria for microglial activation. It has since been discovered that microglia are very active in the healthy brain and therefore, the morphological changes that were associated to activation is rather correspondent to a change in function with microglia possessing many phenotypes (44).

1.4.2 Activation of microglia

As immune effector cells of the CNS, microglia express a wide range of pattern recognition receptors (PRRs) such as toll-like receptors (TLRs), nucleotide-binding oligomerization domains (NODs), NOD-like receptors and scavenger receptors (SRs) to detect and respond to molecular patterns associated with inflammatory stimuli such as Aβ. Upon activation of PRRs microglia undergo physiological and morphological changes to release inflammatory cytokines such as IL-6, TNF-α, IL-1β and IFN-γ which upregulate microglial activation. However, over activation of these cells can lead to neurodegeneration in AD. In the AD brain, sustained accumulation of Aβ induces disease-associated microglia (DAM) via damage-associated molecular patterns (DAMPs). DAMPS facilitate sustained release of pro-inflammatory cytokines and increased production of reactive oxygen species (ROS) and nitric oxide species (NOS) leading to neurodegeneration and further stress on microglia (45, 46, 47). This self-perpetuating cycle of neurotoxicity known as reactive microgliosis is the cause of excessive inflammation and oxidative stress seen in AD (Fig 3). In microglia ROS are primarily generated by NADPH oxidase 2 (NOX2) and activation of this in DAM is associated with DAM signalling, inflammation and Aβ plaque deposition in AD. Brains from AD patients show high expression of inducible nitric oxide synthase (iNOS). Studies show that iNOS deficiency prevents premature mortality, plaque formation, increased Aβ levels and gliosis in AD mice models, which further shows that iNOS induced oxidative stress to be a major instigator of AD pathology (48). On the other hand, neuroprotective markers such as Arginase 1 (Arg-1) have seen to reduce Aβ plaques during sustained neuroinflammation seen in AD. This is through the upregulation of neuroprotective genes such as brain-derived neurotrophic factor (BDNF) and insulin-like growth factor (IGF-1) that promote neuronal survival (49).

1.4.3 'Resting' microglia

Under normal physiological conditions microglial cells function as resident phagocytes with constant surveillance of the CNS rapidly clearing apoptotic cells and debris and protect against injury. In the normal brain, Aβ alone induces microglia with a typically known 'alternative activation' phenotype that induces regulated immune responses that release anti-inflammatory cytokines such as IL-10, IL-4 and TGF-β. These respond to and phagocytose harmful stimuli such as fibrillar Aβ to maintain brain homeostasis and protect the CNS from AD (Fig 3). Expression of amyloid scavenging receptors such as CD36 decrease as defective inflammatory regulation occurs in AD. Microglia in this state can be distinguished by their ramified morphology in which long thin processes extend from the cell soma to scan and survey the

surrounding milieu. Phenotype is characterised by low expression of human leukocyte antigen-antigen D related (HLA-DR) expressed by MHC class II genes expressed by activated microglia as well as cluster of differentiation (CD) molecules such as CD40, CD45 and CD68, whereas microglial marker ionised calcium binding adaptor molecule 1 (IBA-1) can detect resting and activated microglia (50).

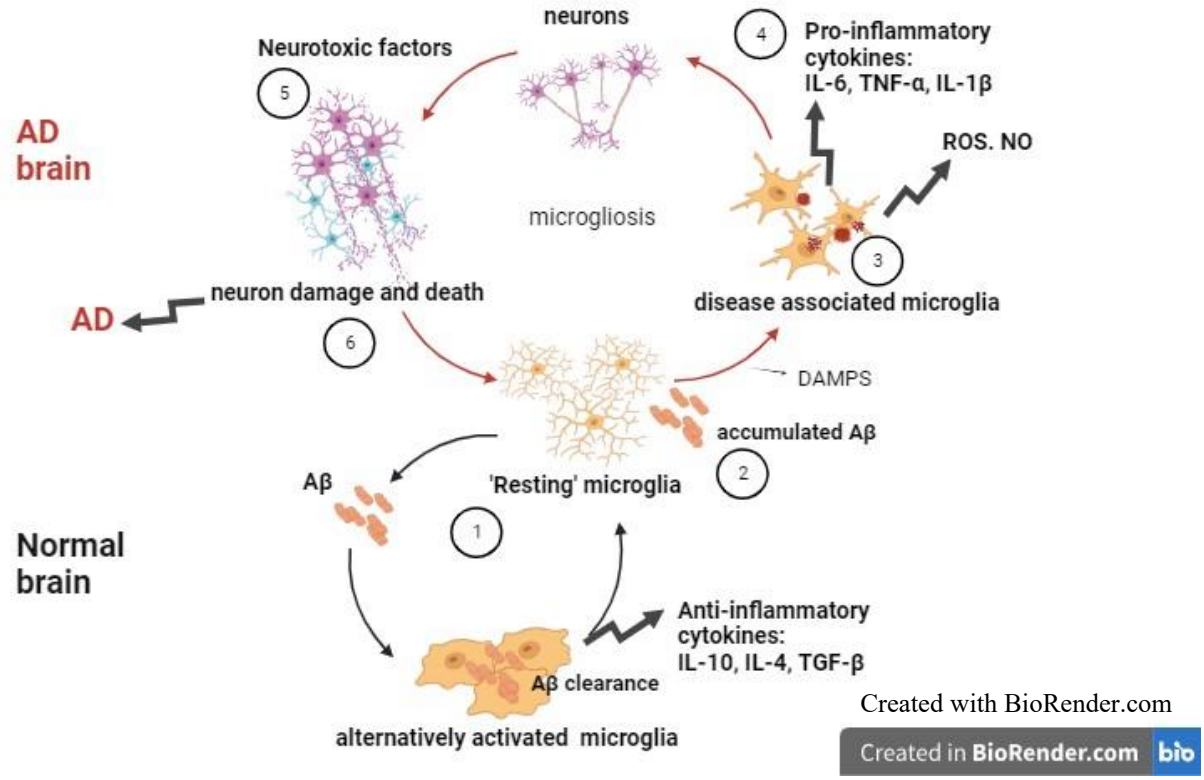

Figure 3. Microglia in the AD brain and normal brain. In normal conditions microglia are alternatively activated to elicit a protective immune response, releasing anti-inflammatory cytokines that target and phagocytose Aβ to prevent its toxic accumulation. In AD, prolonged exposure to Aβ induces disease associated microglia via DAMPS, with sustained activation to release proinflammatory mediators and ROS and NO that lead to neuronal damage and death and chronic neurodegeneration seen in AD.

1.4.4 AD risk associated genes in microglia

Microglia yield high expression of multiple inflammation-associated AD risk associated genes including triggering receptor expressed on myeloid cells 2 (TREM2) with mutations increasing the risk of AD by three-fold (51). TREM2 functions as a pro-inflammatory cell surface receptor that binds and activates adaptor protein DAP12, inducing signal transduction pathways that promote microglia binding and engulfing fibrillised Aβ, APOE and progranulin (PGRN) (an

inflammatory regulator), reducing Aβ aggregation and promoting microglial survival (52, 53). Microglia expressing AD risk associated genes is specific to cell function and activation, suggesting that abnormal activation of these cells contributes to the development of AD rather than being a consequence of AD pathology (54).

Microglial activity is an important factor of AD pathogenesis with studies demonstrating that over-active microglia lose their phagocytic capabilities and can induce a chronic neuroinflammatory environment that promotes Aβ and tau pathology. Thus, targeting microglia may provide potential effective AD therapies whether this be through targeting microglia, microglial modification, immunoreceptors, and inflammatory responses.

1.5 Treatments for AD

Despite scientific breakthroughs over the past several years, there are still no current effective disease modifying therapies for AD. And so consideration of the complex nature of the pathogenesis of AD and investigating repurposed current therapies can lay foundations for the development of novel treatments for AD. AD has a preclinical stage where Aβ deposition can develop in the cortical regions of the brain, although, this precedes the onset of clinical symptoms of up to 20 years. This shows the importance of diagnostic tools for early intervention to administer treatments before irreversible neurodegeneration takes place (55, 56). Further, novel biomarkers have recognised that AD does not have defined clinical stages but rather is a miscellaneous process. This is why identifying specific pathologies and brain changes throughout the disease course will allow us to develop appropriate diagnostic tools and therapies for different stages of the disease (57) (Fig 4).

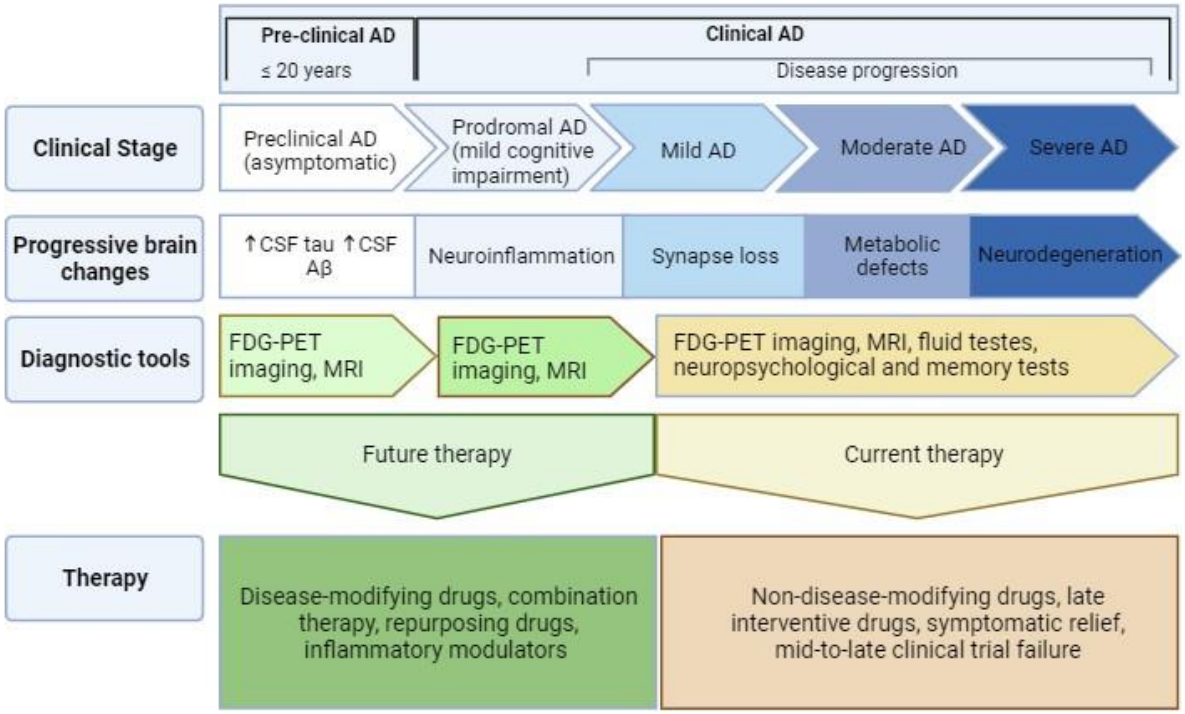

Figure 4. AD represented as a miscellaneous continuum and challenges with developing effective disease-modifying therapies. Pathophysiological changes in the AD brain can precede clinical onset by many years, with clinical onset consisting of many stages ranging from asymptomatic to severely impaired symptoms. In the preclinical stage, progressive Aβ deposition could result in prodromal AD stage, characterized by short-term memory impairment with no effect on day to day living. As disease progresses, many brain areas become affected leading to defective functions resulting in severe memory loss. Despite the lack of AD biomarkers, earlier detection and intervention will ensure that treatments reach patients in an appropriate time. With continuous failed mid-to-late clinical trials, current AD research pipeline requires a shift toward the use of disease-modifying approaches, combination and/or repurposing therapies, and the search for agents selectively targeting specific modulators of inflammation.

1.5.1 Treatments for AD in practice

There are several drugs approved in the UK for AD according to the National Institute for Health and Care Excellence (NICE). Galantamine, rivastigmine and donepezil are cholinesterase inhibitors (ChEIs) recommended to treat mild to moderate AD symptoms. They work to increase the level of acetylcholine (ACh) at synapses to account for the loss from

cholinergic neurons, although, as AD progresses the brain produces less ACh so overtime these drugs will lose their efficacy. While these drugs may delay the early attention and memory deficits seen in AD, they only work to treat symptoms and do not halt disease progression. Lecanemab is a UK approved immunotherapy used to treat mild cognitive impairment or mild dementia caused by AD. It works by targeting soluble aggregated Aβ and works on oligomers and fibrils reducing the amount of Aβ plaques in the brain, slowing cognitive decline in AD patients (58). The UK further approved aducanumab, however this drugs approval has now been suspended according to NICE guidelines due to adverse side effects. Donanemab is a new antibody therapy that binds and destroys (up to 90%) Aβ plaques from the brain, slowing disease progression by 20-30%. It has been said to be the preferred immunotherapy due to management of adverse effects but has yet to be approved by NICE (59, 60).

Memantine is a non-competitive N-methyl-D-aspartate (NMDA) antagonist used to treat people with moderate AD who are intolerant of or have a contraindication to AChE inhibitors or severe AD (61). This drug acts to regulate glutamate levels in the brain, as in AD, glutamate levels increase leading to excessive NMDA receptor activity and neuronal dysfunction and death (62). Despite these drugs it is still essential to research innovative approaches and underlying mechanisms to slow or halt AD progression.

1.6 Nanoclusters

1.6.1 Immunogenic properties of nanoclusters

Nanotechnology is an unconventional modern technology that has shown significant potential in biomedical research and industry (63). It consists of the production of particles ranging in size from 1 to 100 nanometres (nm). Due to their small size, drugs can be easily loaded onto these lipid soluble nanoparticles (NPs) and transported to various biological sites. With their biocompatible and durable nature, they are able to project the drugs maximum therapeutic effect through enhanced solubility and specificity. Research has shown these NPs to have immunogenic properties and hence have use in vaccine delivery and cancer treatments (64). Their capability to modulate immune response means they can be used to treat neurodegenerative disorders like AD. Studies have demonstrated some NPs to inhibit Aβ fibrilisation and have the potential to transport drugs across the BBB (65, 66, 67).

1.6.2 Lysozyme-encapsulated gold nanoclusters as a therapeutic agent for AD

NPs and nanoclusters (NCs) are both nanoscale materials, but they typically differ in composition, structure and properties. NPs are generally more uniform in shape and are used in biomedical applications to enhance the performance of certain materials, catalyse chemical reactions, and harness drugs. NCs are groups of atoms, molecules or ions with a diameter measuring between 2 and 50nm with a non-uniform structure and are frequently used for their optical and physiochemical properties (68, 69). Lysozyme-encapsulated gold nanoclusters (Lys-AuNCs) have sparked interest in the research field due to their specific fluorescence properties and sustainable synthesis methods using proteins as growth scaffolds. Gold is an advantageous inert noble metal with adequate biocompatibility and sustainability in various biomedical applications and hence is used in accompaniment with nanocluster synthesis. Lys-AuNCs have attractive properties such as displaying quantum mechanical characteristics due to their small diameter (of < 2nm) and small clusters of up to 100 gold atoms proving to be highly stable, non-photobleaching and have prolonged fluorescence emission in the infrared spectrum (70). Lys-AuNCs are also non—toxic, maintaining protein function post synthesis, have a well-controlled size and surface functionalisation and so can be used in various biomedical applications. Lysozyme, a protein able to form amyloid fibrils is used as a growth scaffold for AuNCs and works to reduce and stabilise gold ion precursors in AuNCs in the ‘one pot process’ forming lysozyme-stabilised AuNCs (71). Metal based particles are used for various biomedical applications and have shown to induce important innate and adaptive immune responses that play a pivotal role in the development of neurodegenerative diseases such as AD (72). Recent studies have also shown these novel particles to inhibit the synthesis of Aβ plaques *in vitro* (73).

1.7 Hypothesis and aims

Lys-AuNCs have been shown to inhibit the fibrillation of Aβ in vitro as well as induce important innate and adaptive immune responses that play a role in the development and progression of AD (74, 75). Microglial-mediated immune responses have shown to regulate or exacerbate Aβ pathology and neuroinflammation in AD. It can therefore be hypothesised that treatment with Lys-AuNCs may modulate microglial-mediated immune responses to reduce AD pathology providing a potential therapy for AD. This study aims to investigate the immunogenic properties of Lys-AuNCs on microglial cells and the associated mechanisms that affect AD pathology: Specific objectives are:

i) To characterise and validate the Lys-AuNCs to maintain consistency between batches.

ii) To assess the toxicity of Lys-AuNCs in HMC3 microglial cells using an MTT assay.

iii) To investigate the localisation of Lys-AuNCs in HMC3 cells.

iv) To determine if Lys-AuNCs modulate microglial phenotype through examining cell morphology and quantifying pro-inflammatory and anti-inflammatory marker expression.

2. Materials and methods

2.1 Table of reagents

Various antibodies and reagents were used for experiments, all of which were used in accordance with the supplier's protocol (Table 1).

Table 1. List of reagents suppliers and catalogue numbers.

Ab or reagent	Company	Cat No
Acetone	VWR Chemicals	
Bovine serum albumin (BSA-AuNCs)	Sigma Aldrich	A4503-100G
DMEM (1X) Dulbecco's Modified Eagle Medium	Fisher Scientific	11965084
DMSO	Fisher Scientific	D-1391
Ethanol	VWR Chemicals	
Fetal bovine serum (FBS)	Fisher Scientific	10500064
Gibco™ L-glutamine (200mM)	Fisher Scientific	11539876
Gibco™ Penicillin Streptomycin (10,000 U/mL)	Fisher Scientific	11548876
Gibco™ TryplE™ Express Enzyme (1X), no phenol red	Fisher Scientific	10718463
Heat-inactivated FBS	Gibco	11550356
Hydrogen peroxide solution (H2O2)	Sigma Aldrich	H1009-100ML
Hydrophobic Barrier Pap pen	Fisher Scientific	R3777
Immedge wax pen	Vector Labs	
L-glutamine	Gibco	25030081
Lipopolysaccharide (LPS) from *S. enterica*	Sigma Aldrich	L7011-100MG
Lysozyme (lyophilised powder from chicken egg white)	Sigma Aldrich	L6876-5G

MEM Non-Essential Amino Acids Solution (100X)	Fisher Scientific	11140050
MTT (3-(4,5-Dimethylthiazol-2-yl)-2,5-Diphenyltetrazolium Bromide)	Fisher Scientific	M6494
OCT mounting medium	VWR chemicals	36163E
Paraformaldehyde (PFA) 4%	Fisher Scientific	J19943.K2
Penicillin/Streptomycin	Sigma Aldrich	
Potassium phosphate monobasic (KH_2PO_4)	Sigma Aldrich	P5655-500G
Sulphuric acid (H2SO4; 1 M)	Honeywell	1M-35276-16
Thermo Scientific™ Oxoid™ Phosphate Buffered Saline Tablets	Fisher Scientific	10209252
TMB Substrate Solution	Invitrogen	88-7064-88
Tris base	Fisher Scientific	M-27435
Triton-X-100	Fisher Scientific	85111
Trypan Blue Stain (0.4%)	Fisher Scientific	15250061
TrypLE Express Enzyme	Thermo Fisher	
Tween-20	VWR Chemicals	437082
Vectasheild mounting media (with DAPI)	Vector Labs	H-1500
VECTASHIELD HardSet Antifade mounting medium	2BScientific	H-1400

2.2 Buffers and solutions

All buffers and solutions necessary for experiments were made with descriptions listed below.

Complete Dulbecco's Modified Eagle Medium (c-DMEM)

50 mL of heat-inactivated fetal bovine serum (FBS) (10%), 5.5 mL penicillin streptomycin (1%), 5.5 mL non-essential amino acids (NEAAs) (1%) and 11 mL of L-glutamine (2%) added to 500 mL of Dulbecco's modified Eagle Medium (DMEM).

10x phosphate buffer saline (PBS)

Make 1 L stock solution by dissolving 17.8 g of Na_2HPO_4, 2.4 g of KH_2PO_4, 80 g of NaCl, 2 g of KCl, in 1 L of DiH2O adjusting the pH of the buffer by adding sodium hydroxide (NaOH) until it reads 7.4 on the pH meter. If it goes above 7.4 add hydrochloric acid (HCL) to bring it down. 1x PBS stock solution made by adding 100mL of 10xPBS to 900mL DiH2O.

1x PBS Tween (PBST)

To prepare I L, 0.5 mL of Tween-20 (0.05%) added to 100 mL 10x PBS in 900 mL DH_2O and mixed.

Immunocytochemistry staining blocking buffer

1 g of bovine serum albumin (BSA) (1%) dissolved in 100mL of 1 x PBS divided into 10mL aliquots.

Triton-X-100

Add 75µL of Triton-X to 30mL 1xPBS to make 0.25% Triton-X.

2.3 Synthesis and characterisation of Lys-AuNCs and BSA-AuNCs

Lys-AuNCs were prepared using a modified one-pot process with lysozyme (crystallized and lyophilized powder, from chicken egg white (HEWL), ≥99%) and Gold (III) Chloride Hydrate purchased from Sigma Aldrich and PBS tablets were used to make 1XPBS. A 5 mL solution of 10mg/mL lysozyme was mixed with a 5 mL solution of 4mM $HAuCl_4$ and 5mL of sterile pre-warmed DiH_2O was added and solution was incubated at 37ºC for 5 minutes. 0.5 mL of 1M NaOH was added and incubated in water maintained at 36-39ºC for 7 hours with

continuous stirring then moved to a 37ºC incubator for 48 hours (no stirring). Lys-AuNCs were then dialysed using a 10kDa dialysis cassette submerged in 1XPBS to remove any impurities from the solution (with continuous stirring). 5mL of the Lys-AuNC solution was then filtered through a 0.22 μm syringe filter to remove any microbial contaminants. Viability characteristics of the Lys-AuNCs were assessed through measuring fluorescence emission spectra using a Jobin Yvon HORIBA Fluorolog 3.

BSA-AuNCs were prepared by adding 5 mL of 10 mM $HAuCl_4$ solution to 5 mL of 50mg/mL BSA solution and 5 mL pre-warmed DiH_2O and incubating solution on a hotplate for 2 minutes. 0.5 mL of 1M NaOH was added to the BSA-AuNC solution sealing with parafilm and wrapping in tinfoil to omit light and submerging in water maintained at 36-39ºC with continuous stirring. After 6-hour incubation BSA-AuNC universal is transferred to a 37ºC incubator overnight (no stirring). BSA-AuNCs are then dialysed using a 10kDa dialysis cassette submerged in 1XPBS to remove any impurities from the solution (with continuous stirring). 5mL of the BSA-AuNC solution was then filtered through a 0.22 μm syringe filter to remove any microbial contaminants. Viability characteristics of the BSA-AuNCs were assessed through measuring fluorescence emission spectra using a Jobin Yvon HORIBA Fluorolog 3.

NCs are synthesised every few months for use in ongoing experiments and to ensure optical and physiochemical properties of the Lys-AuNCs remain intact through the synthesis process, the concentration of Lys-AuNCs must be comparable to previous batches. 3 serial dilutions were made from the remaining pre-dialysed Lys-AuNCs solution (1:10, 1:100 and 1:1000) from synthesis, and fluorescence intensity measured at each dilution (using a UV-Vis spectrophotometer) at 280nm. Readings were plotted as a concentration curve and equation of line used to calculate the concentration of NCs following dialysis from the filtered Lys-AuNCs measured at a dilution of 1:10 (also read at 280nm). The same process was completed for BSA-AuNCs.

2.4 HMC3 cell line and maintenance in culture

The human microglial clone 3 cell line (HMC3) was established by Prof. Tardieu in 1995 through SV40 immortalisation of human microglial cells. They isolated the microglial cells by circular shaking from primary mixed cultures of human spinal cord and cortical cells derived from 8–12-week-old embryos and kept in vitro for 10-15 days. The cells were then immortalized by transfection of the SV40 T antigen in primary human microglial cultures,

derived from 8- to 10-week-old embryos (66). It should also be pointed out that primary CNS cultures are not necessarily restricted to parenchymal microglia, and other myeloid populations may be present in these cultures, possibly contributing to the culture heterogeneity.

All cell culture procedures are performed in a laminar flow cabinet to protect workspace samples from contamination. HMC3 cells are stored in 1mL vials at -80ºC or liquid nitrogen (LN_2). Cells are thawed in 37ºC water bath for 1 minute, liquid is then removed from the vial and transferred to a T25 flask with volume made up to 5mL with 3 mL c-DMEM and 1mL heat inactivated FBS where it is incubated overnight at 37ºC, 5% CO_2 and replaced with 5mL pre-warmed c-DMEM the following day. Once reached 70-90% confluency the cells are split into a T75 flask where they are subsequently split every 2-4 days depending on the dilution. To split cells the old media is removed from the flask and washed with 3mL of PBS then trypsinised with 3 mL of TrypLE Express enzyme and incubated at 37ºC, 5% CO_2 to detach the cells. Cells are viewed under a microscope to ensure all cells have detached before resuspending with 7mL of c-DMEM which inactivates the TrypLE to avoid digestion of the cells. When seeding cells into plates following resuspension, cells are centrifuged at 1400 r.p.m for 5 minutes to concentrate cells to a pellet. Cell supernatant is removed (avoiding disturbance of the pellet) and 10mL c-DMEM is added pipetting up and down until the cell pellet is completely resuspended providing a single cell suspension to be seeded into plates.

2.5 Growth curve for HMC3s

In order to evaluate the growth characteristics of HMC3 cells a growth curve was generated by harvesting and counting cells to seed at a density of $2x10^3$ cells per cm^2 of 5 T25 flasks with duplicate plates counted each day over 5 days (n=2). Duplicate cell counts were averaged and plotted on a log-linear scale and population doubling time determined by identification of the cell number at the exponential phase (trace curve until number has doubled) and calculating the time between the two points using the doubling time equation (**Doubling time (DT)= duration (hrs) * log2 / log(current density) – log(initial density**).

2.6 HMC3 cell viability assay

In order to assess the toxicity of the Lys-AuNCs on microglial cells a MTT assay was performed to measure HMC3 cell viability based on the reduction of yellow tetrazolium salt (3-(4,5-dimethylthiazol-2-yl)-2,5-diphenyltetrazolium bromide or MTT) to purple formazan crystals by metabolically active cells. HMC3 cells were cultured and seeded into a 96-well

plate at a density of 8000 cells per well with final wells containing 100µL of c-DMEM and incubated at 37ºC, 5% CO_2 for 24 hours. After 24 hours the old media was aspirated from the wells and replaced with media treated with Lys-AuNCs or lysozyme and BSA-AuNCs as nanocluster controls at concentrations of 50, 200, 400 and 600µg/mL for 24, 48 and 72 hours. Nanoclusters require a stabilising agent such as lysozyme or BSA to prevent aggregation. Treating with lysozyme alone accounts for any protein induced effects and BSA-AuNCs provides a control for the gold as these are distinct from Lys-AuNCs. Plates were then imaged using an Thermo Fisher Scientific EVOS FL AUTO microscope at x 20 magnification to assess any Lys-AuNC induced morphological changes.

Cells were also treated with 1 µg/mL of LPS (*S. enterica*) to confirm induced microglial response. Untreated cells (UT) were used as a positive control and cells treated with H2O2 were used as a negative control for toxicity which inhibited HMC3 cell growth at ~500 µg/mL. Following each time point the treated media was aspirated from wells and 90 µL of c-DMEM and 10 µL of 10mM MTT was added to wells to make a final well concentration of 1mM. The plate was covered in foil to omit light and incubated at 37ºC, 5% CO_2 for 2 hours. The media was then removed from wells and 100 mL of DMSO added to each well and plate carefully tapped to resuspend the formazan crystals. Plate is covered in foil and incubated at 37ºC, 5% CO_2 for a further 5 minutes then plate read on Flexstation plate reader at 570nm. Wells containing media only were included as blanks and measured and subtracted from all values to account for any background absorbance.

2.7 Immunocytochemistry

Coverslips were added to wells of a 24 well plate and cells were seeded at $1x10^5$ cells/well in c-DMEM in and incubated at 37ºC 5% CO_2 for 24 hours. Cells were then treated with Lys-AuNCs and relevant control treatments lysozyme and BSA-AuNCs for 24 hours at concentrations 5, 10, 50, 200 µg/mL, and cells treated with 1 µg/mL LPS were used as a positive control and cells left untreated as a normalised control. Plates were incubated for 24 hours at 37ºC 5% CO_2. Spent media was removed from each well and cells were washed with PBS then fixed (with 4% PFA) and permeabilised (using Triton-X-100). Cells were then blocked with BB for 30 minutes at RT prior to relevant primary antibodies diluted in BB being added and incubated overnight at 4ºC. The following day cells were washed and blocked before administering corresponding fluorophore conjugated antibodies and incubating for 1 hour at RT in a light omitting box. Cells were then washed and stained with DAPI for 5 minutes at RT

before mounting coverslips using hard-set antifade mounting media to slides. Images were taken on a Leica SP8 Confocal microscope with images taken at x 63 objective.

Table 2. List of antibodies used for ICC-F experiments with suppliers and catalogue numbers.

Abs or immunostaining reagents	Final dilution used	Final concentration of Ab used	Company	Cat No
Immunocytochemistry				
DAPI (4′,6-diamidino-2-phenylindole, dihydrochloride)	1:1000	1 µg/mL	Fisher Scientific	62248
IBA1 antibody (Guinea pig monoclonal recombinant IgG)	1:100	10 µg/mL	Synaptic Systems	234 308
NOS2 antibody (C-19)	1:500	0.4 µg/mL	Santa Cruz Biotechnology	sc-649
Arginase 1 (Arg-1) antibody (N-20)	1:100	2 µg/mL	Santa Cruz Biotechnology	Sc-18351
Alexa Flour™ 488 donkey anti-rabbit IgG (H+L)	1:1000	2 µg/mL	Fisher Scientific	A21206
Alexa Flour™ 555 goat anti-rat IgG (H+L)	1:1000	2 µg/mL	Fisher Scientific	A21434

2.8 Quantification of inflammatory marker expression in HMC3 cells

Quantification of iNOS and arg-1 expression in HMC3 cells was completed by processing fluorescent images on imageJ by merging DAPI and FITC channels to create a merged image and applying scale bars (25µM). Each cell was highlighted using the drawing tool as a region of interest and measuring the area, mean grey value and integrated density. Corrected total cell

fluorescence (CTCF) was calculated by taking the integrated density and subtracting the area multiplied by the mean fluorescence of background readings. 4 images were taken per treatment and the mean CTCF was taken from each and plotted on bar graphs with statistical significance on GraphPad Prism Software 8.0.2. To avoid quantification bias 4 consistent areas were marked on each sample slide with an image taken from each area on a confocal Lecia SP8 microscope at 63 x objective.

2.9 Statistical analysis

All data is represented by mean ± SEM with statistical significance determined using ordinary one-way ANOVA with Tukey's post hoc test via GraphPad Prism 8.0 software with *p* values of < 0.05 being significant.

3. Results

3.1 Synthesis of Lys-AuNCs and viability characterisation

Since we are working with cell culture the Lys-AuNCs must be sterile to prevent any contamination with the HMC3s. To ensure there are no abnormalities in terms of nanocluster structure which could in turn affect their physiochemical properties we characterise their fluorescent properties by measuring fluorescence intensity from a collected sample of the filtered Lys-AuNCs and measuring their fluorescence intensity (FI) after excitation at 470nm using a Jobin Yvon HORIBA Fluorolog 3 to confirm their optical properties (Fig 5). 3 subsequent FI measurements were taken at each emission wavelength ranging from 500-800nm with average FI values plotted as a curve using GraphPad Prism 8.0. Results showed when Lys-AuNCs were excited at 470 nm they emitted in the red-shift at a wavelength of 680 nm with fluorescent intensity (FI) peak measured at 6.17 x 10^6 a.u. . Fluorescence lifetime readings were also measured using a UV-Vis spectrophotometer with peak measured at 280 nm to confirm the newly synthesised NCs were not NPs.

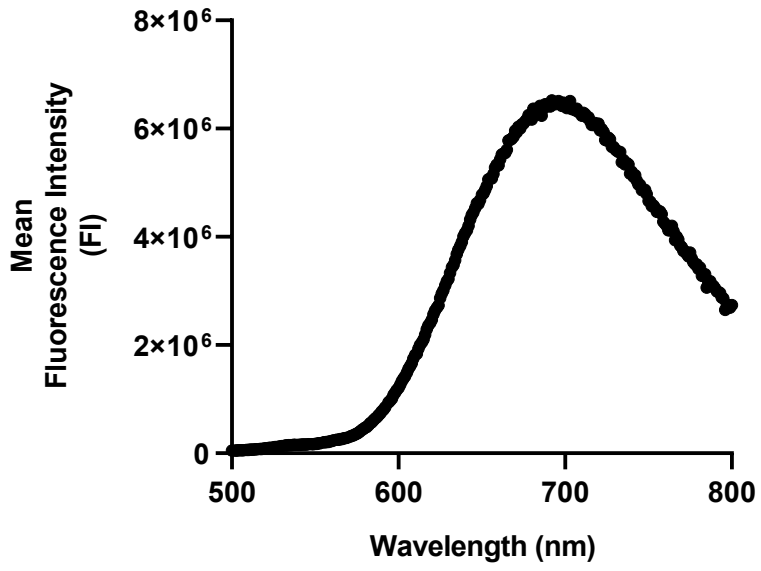

Figure 5. Fluorescence intensity measurements of Lys-AuNCs confirm they emit in the red-shift when excited at 470 nm. After synthesis and filtration 5 mL of the Lys-AuNC stock solution was taken and excited at 470nm on a HORIBA Fluorolog 3 and fluorescence intensity measurements were recorded, averaged, and plotted as a curve.

In order to maintain consistency in concentration of NCs between batches a concentration curve was generated to confirm the NCs optical and physiochemical properties by relating concentration of pre-dialysed clusters to that of filtered clusters (Fig 6A-D). A sample was taken from the remaining pre-dialysed Lys-AuNCs as a representative of the starting concentration of Lys-AuNCs (no loss through dialysis). 3 serial dilutions were made from the sample, first diluting 1:10 taking 300 µL of sample and diluting in 2700 µL PBS, the sample was diluted 1:10 a further 2 times (1:100 and 1:1000) and absorbance measured at each dilution at 280nm on a UV-Vis spectrophotometer. For the current batch the molar concentration of Lys-AuNC solution was calculated at 22.6µM (Fig 6A). This was used as our 1:10 dilution and corresponding concentrations (2.26 for 1:100 and 0.226 for 1:1000) plotted against absorbance measurements (read at 280nm) on excel to get our concentration curve where the equation of line is used to confirm the concentration of filtered Lys-AuNCs by subbing in the absorbance value (1.04975) of filtered Lys-AuNCs measured at 280 nm (at a 1:10 dilution) giving a resulting concentration of 2.95 mg/mL (Fig 6B). The molar concentration was calculated for BSA-AuNCs as before at 35.8 µM (Fig 6C). The same process was completed for BSA-AuNCs with filtered absorbance value at 2.9876 (280 nm) subbed into the equation of line from the concentration curve calculated the concentration of filtered BSA-AuNCs at 27.38 mg/mL (Fig 6D).

A

MW of Lys = 14300 g/mol

TV =15.5mL (0.0155 L)

(0.0155 * 14300 = 221.65)

= 0.05 / 221.65 = 0.000226

= 0.000226M = 0.226mM = **22.6µM**

Conc (µM)	OD @ 280nm
35.84	2.5712
3.584	0.2766
0.3584	0.0439

B

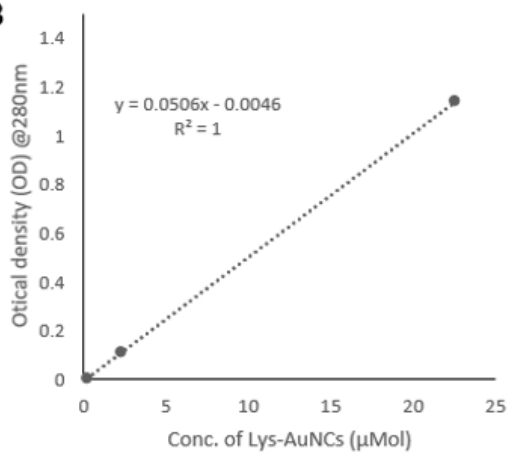

y= mx + c

y= 0.0506x + 0.0046

x= 1.04975 - 0.0046/0.0506

x= 20.66 µM

= 206.6 µM before 1:10 dilution

=0.2066 mM = 0.0002066 M *14300 = **2.95 mg/mL**

C

MW of BSA = 66430.3 g/mol

TV =10.5mL (0.0105 L)

(0.0105 * 66430.3 = 697.52)

= 0.25 / 697.52 = 0.000358

= 0.000358M = 0.358mM = **35.8µM**

Conc (µM)	OD @ 280nm
22.6	1.1389
2.26	0.11285
0.226	0.004

D

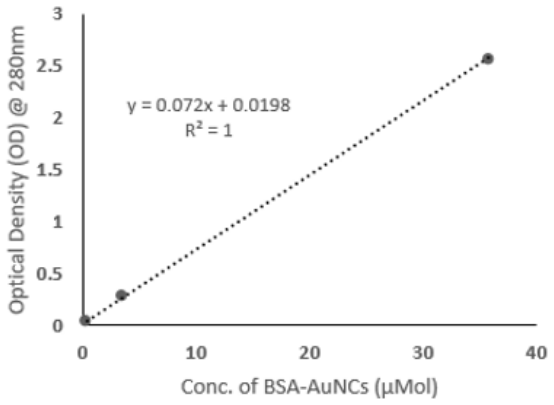

y= mx + c

y= 0.072x + 0.0198

x= 2.9876 - 0.0198/0.072

x= 41.22 µM

= 412.2 µM before 1:10 dilution

=0.4122 mM = 0.0004122 M *66430.3 = **27.38 mg/mL**

Figure 6. Calibration curve relating concentration of pre-dialysed NCs with filtered NCs confirmed their optical and physiochemical properties. A-D 3 dilutions of 1:10, 1:100, 1:1000 were prepared from pre-dialysed Lys-AuNC and BSA-AuNC solution and absorbance was read at each dilution on UV-Vis spectrophotometer at 280 nm. The molar concentration of NCs was calculated prior to dilution and used as the 1:10 measurement and filtered concentration of NCs calculated from resulting line equation (y = mx + c).

3.2 HMC3 doubling time to establish growth rate

In order to assess the immunomodulatory properties of Lys-AuNCs on HMC3s experiments span over a time period varying from 1-3 days to assess immune responses at different time points, it is therefore essential that cells are seeded at appropriate densities for transduction with Lys-AuNCs. Cells were seeded into 10 T25 flasks and counted in duplicate (n=2) each day with the average count plotted against time as a curve on a logarithmic scale (Fig 7A). The current density of HMC3 cells was measured at 1.925 x 10^5 cells/ mL and initial density at 4.5 x 10^4 cells/ mL with doubling time calculated at 22.9 hours using the calculated equation (Fig 7B).

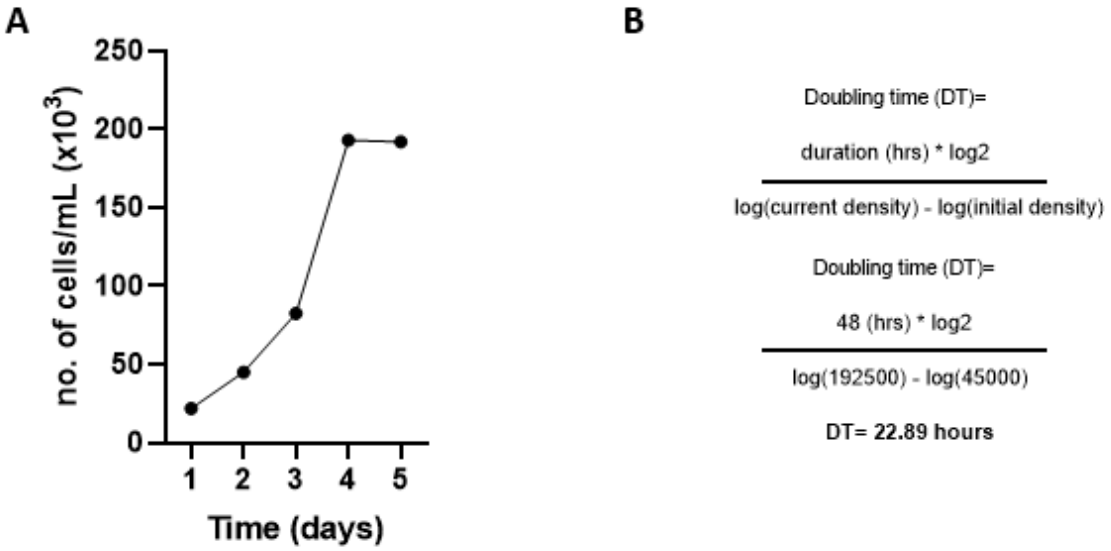

Figure 7. Growth curve to establish doubling time of HMC3s for seeding densities. (A) Cells were seeded at 10 x 10^3 cells/ mL in 10 T25 flasks (n=2) and cell numbers were counted daily (using a haemocytometer) over 5 days. Counts were used to plot growth curve to establish exponential growth phase of HMC3s and doubling time was then calculated using the following equation (B).

3.3 MTT viability Assay to assess the toxicity of Lys-AuNCs

To determine potential cytotoxic effects of the Lys-AuNCs we assessed viability of HMC3s after treatment via an MTT assay. HMC3 cells were treated with varying concentrations of Lys-AuNCs, Lysozyme and BSA-AuNCs. Untreated cells (UT) were used as a positive control and cells treated with H_2O_2 were used as a negative control for toxicity. Our results show UT cells with 100% viability after 24, 48 and 72 hours of incubation. When treated with lysozyme at concentrations of 50-400 µg/mL, HMC3 cells showed no significant change in viability at 24, 48 and 72 hours, compared to UT controls. However, when treated with 600 µg/mL HMC3 cells showed a significant decrease in viability at both 48 hours (-79.9%; *p<0.05) and 72 hours (-69.9%;*p<0.05). HMC3 cells treated with BSA-AuNCs at concentrations 50-600 µg/mL showed no significant change in viability at 24 and 48 hours compared to UT controls but induced a significant decrease in viability at 400 µg/mL (-77.9%, *p<0.05) and at 600 µg/mL (-73.7%, *p<0.05) at 72 hours. Finally, when treated with Lys-AuNCs at concentrations of 50-600 µg/mL, HMC3s showed no significant change in viability over 24 and 48 hours but when treated with 600 µg/mL, cells displayed a significant decrease in viability at 72 hours compared to UT controls (-88.9%, *p<0.05) (Fig 8).

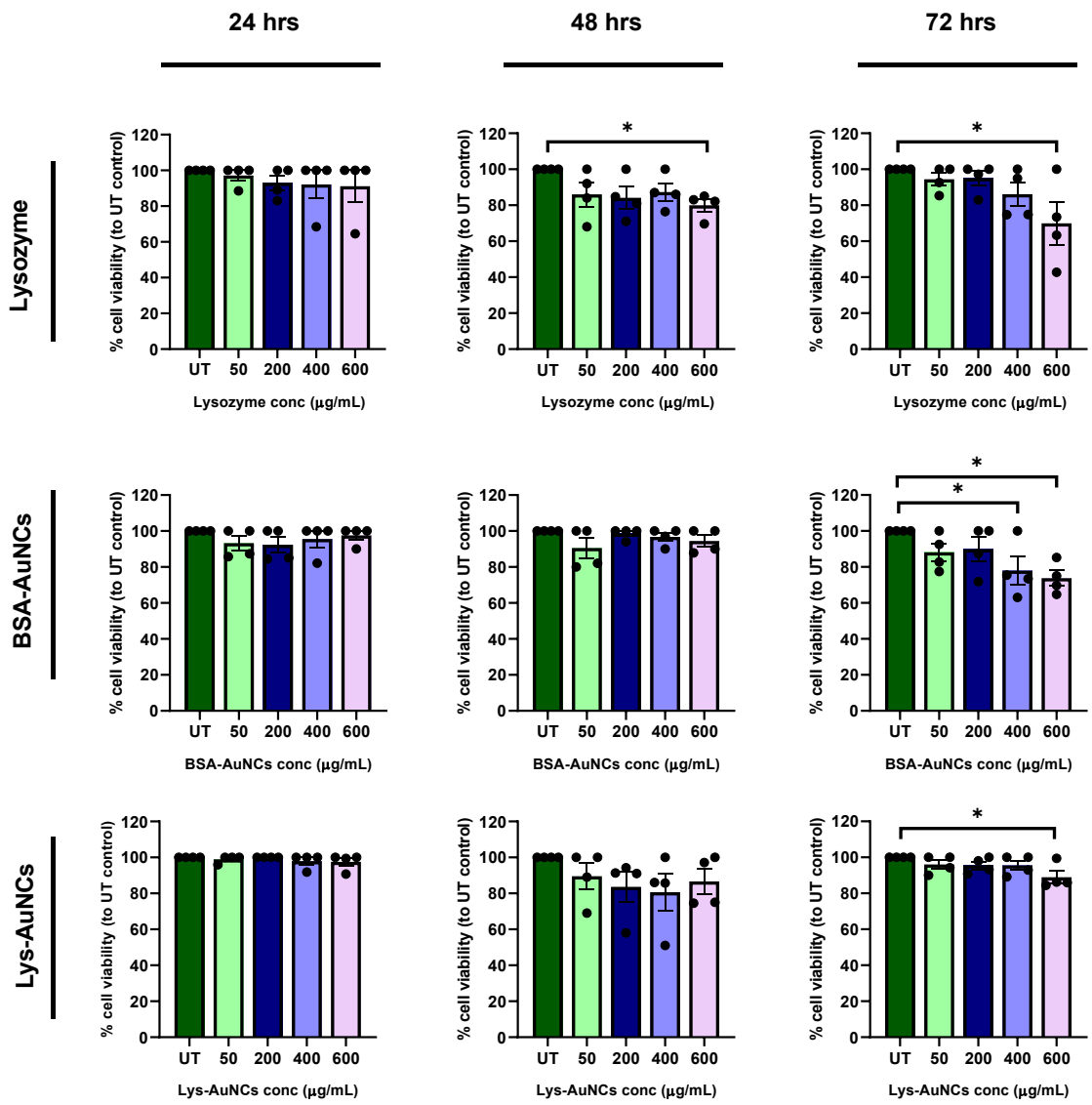

Figure 8. Assessing toxicity of Lys-AuNCs on HMC3 cells via MTT viability assay. HMC3 cells were seeded at $8x10^3$ cells/well in a 96-well plate and treated with concentrations ranging from 50-600 µg/ mL of lysozyme, Lys-AuNCs and BSA-AuNCs and incubated at 24, 48 and 72 hours. An MTT assay was then used to assess cell viability. Data is presented as mean ± SEM and statistical significance determined using ONE-way ANOVA on GraphPad Prism 8.0, *p<0.05. (n=4 independent experiments).

3.4 Localisation of Lys-AuNCs in HMC3 cells

Since we are investigating modulatory effects of Lys-AuNCs on HMC3 cells we sought to assess where the Lys-AuNCs are exerting these potential effects by establishing intracellular or extracellular localisation. HMC3 cells were treated with 50 µg/mL of Lys-AuNCs and BSA-

AuNCs as an experimental control and cells were left untreated as a control for 24 hours. ICC staining was performed staining treated samples with DAPI a nuclear stain and Lys-AuNCs were visualised as they emit their own fluorescence in the infrared spectrum (@ 670nm). Images were taken on a confocal Leica SP8 microscope at x 63 magnification. Results showed cellular localisation of Lys-AuNCs in HMC3 cells, however this requires further validation such as a cytoskeletal stain to visualise the nanolcusters in the cell (Fig 9).

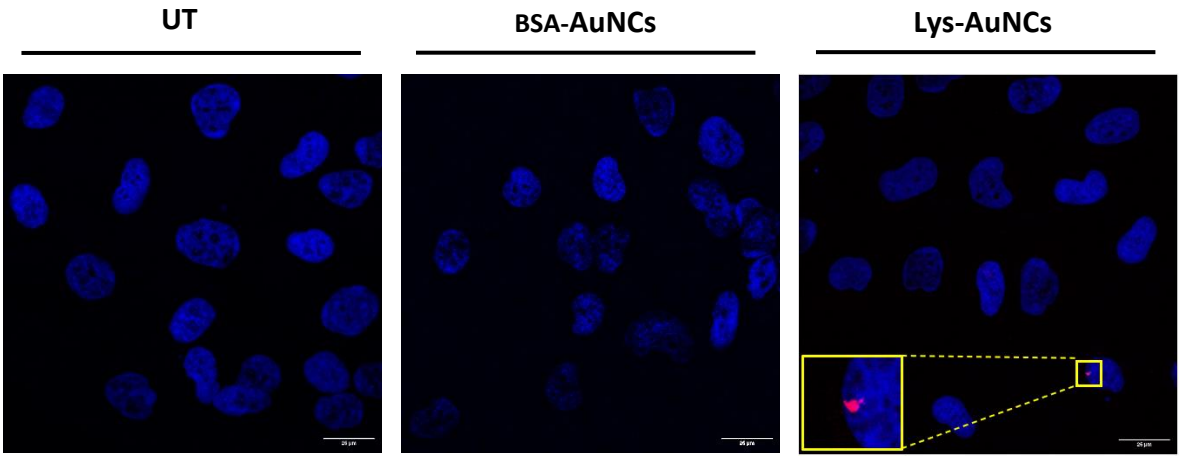

Figure 9. Lys-AuNCs show cellular localisation in HMC3 cells. HMC3s were seeded at 10,000 cells/ mL on glass coverslips for 24 h (at 37ºC, 5% CO_2) then treated with 50 µg/mL of Lys-AuNCs and BSA-AuNCs as a control and incubated as before for a further 24 hours. Cells treated with 0 µg/ mL (UT) as a control. Cells were stained with a nuclear stain DAPI (blue fluorescence) and Lys-AuNCs emit their own fluorescence in the red-shift. Images (1024 x 1024 pixels) were taken on a confocal Leica SP8 microscope at x 63 magnification and merged using ImageJ software. Scale bar 25µM.

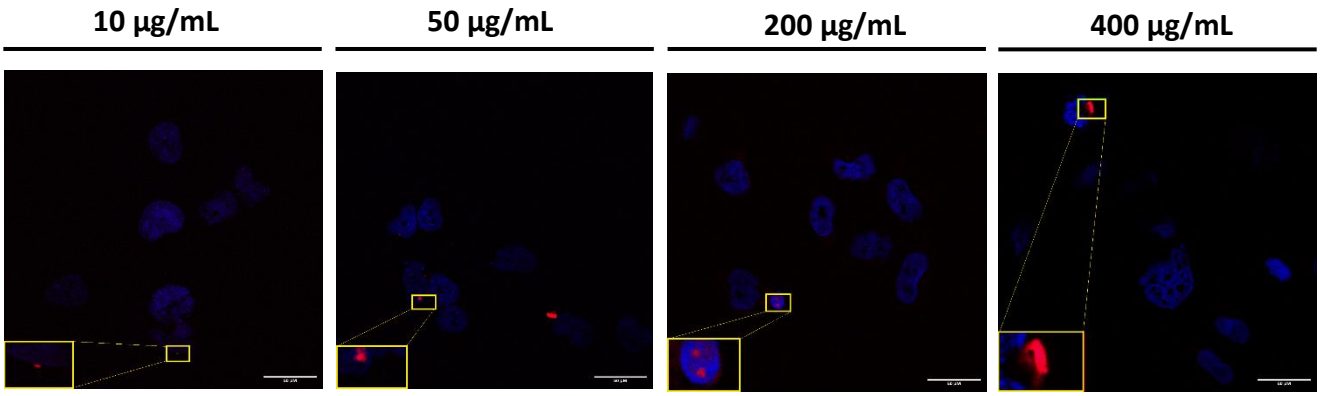

Figure 10. Lys-AuNCs show intracellular localisation in HMC3 cells through Z-stack image analysis. HMC3s were seeded at 10,000 cells/ mL on glass coverslips for 24 h (at 37ºC, 5% CO_2), then treated with 10, 50, 200 and 400 µg/mL of Lys-AuNCs and BSA-AuNCs as a control and incubated as before for a further 24 hours. Cells were stained with a nuclear stain DAPI (blue fluorescence) and Lys-AuNCs emit their own fluorescence in the red-shift. Images (1024 x 1024 pixels) were taken on a confocal Leica SP8 microscope at x 63 magnification and merged using ImageJ software. Scale bar 25µM.

We further validated the previous results by treating HMC3 cells with more concentrations including 10, 50, 200 and 400 µg/mL of Lys-AuNCs and corresponding BSA-AuNCs as an experimental control and cells were left untreated as a control. Z-stack images were taken on a confocal Leica SP8 microscope at x 63 magnification which produce 3D images of a cell. Results showed intracellular localisation of Lys-AuNCs in HMC3 cells treated with 50 µg/mL and 200 µg/mL (Fig 10).

3.5 Morphology changes of HMC3 cells induced by Lys-AuNCs

Microglial cells are exceptionally diverse in their morphological characteristics which is correlated to their diverse functionality, we sought to evaluate morphology changes of HMC3 cells induced by Lys-AuNCs. Cells were seeded at 8000 cells/mL and incubated for 24 hours then treated with various concentrations of Lys-AuNCs, lysozyme and BSA-AuNCs (50, 200, 400 and 600 µg/mL) and incubated for a further 24 hours. Cells were also treated with LPS as a positive control to assess morphology changes of the HMC3s following pro-inflammatory stimulation. Phase images were taken on an eVOS FL Auto microscope at x 20 objective with images processed through ImageJ software. HMC3 cells left untreated show typical ‘resting’

morphology with small cell bodies and fine ramified processes that allow for the scanning of the local brain environment for pathogens and cellular damage (Fig 11). HMC3s stimulated with LPS have formed an activated phenotype with visibly enlarged cell somas and retracted thicker processes due to the initiation of immune responses in response to pro-inflammatory stimuli (LPS) (Fig 12).

HMC3 cells did not display any marked signs of activation when treated with concentrations of lysozyme and BSA-AuNCs and generally displayed typical 'resting' morphology with ramified shape, small cell bodies and fine processes (Fig 12B & C). Although when treated with 200 µg/mL of lysozyme cells displayed more activated morphology with enlarged cell somas (Fig 12B). Although not marked, cells treated with Lys-AuNCs did show slightly more activated morphology across all concentrations with enlarged cell bodies and thicker process (Fig 12D).

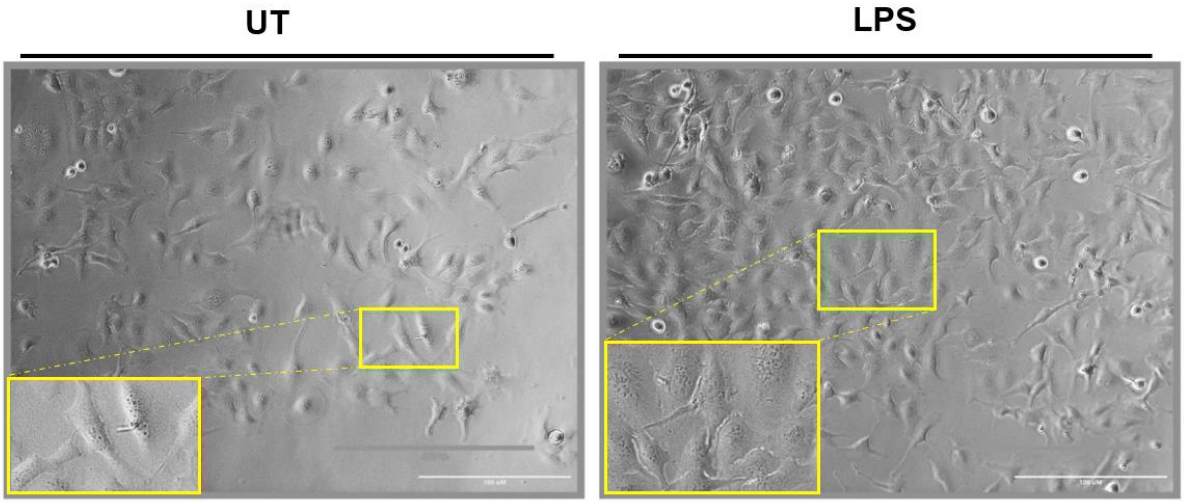

Figure 11. HMC3 cells show activated morphology following pro-inflammatory stimulation. HMC3 cells were seeded at 8000 cells/ mL and incubated (at 37ºC, 5% CO_2) for 24 hours then treated with 1 µg/mL lipopolysaccharide (LPS) from *S. enterica* and incubated as before for a further 24 hours. Phase images were taken using an EVOS FL AUTO microscope at x 20 magnification (n=3). Scale bar 400 µM.

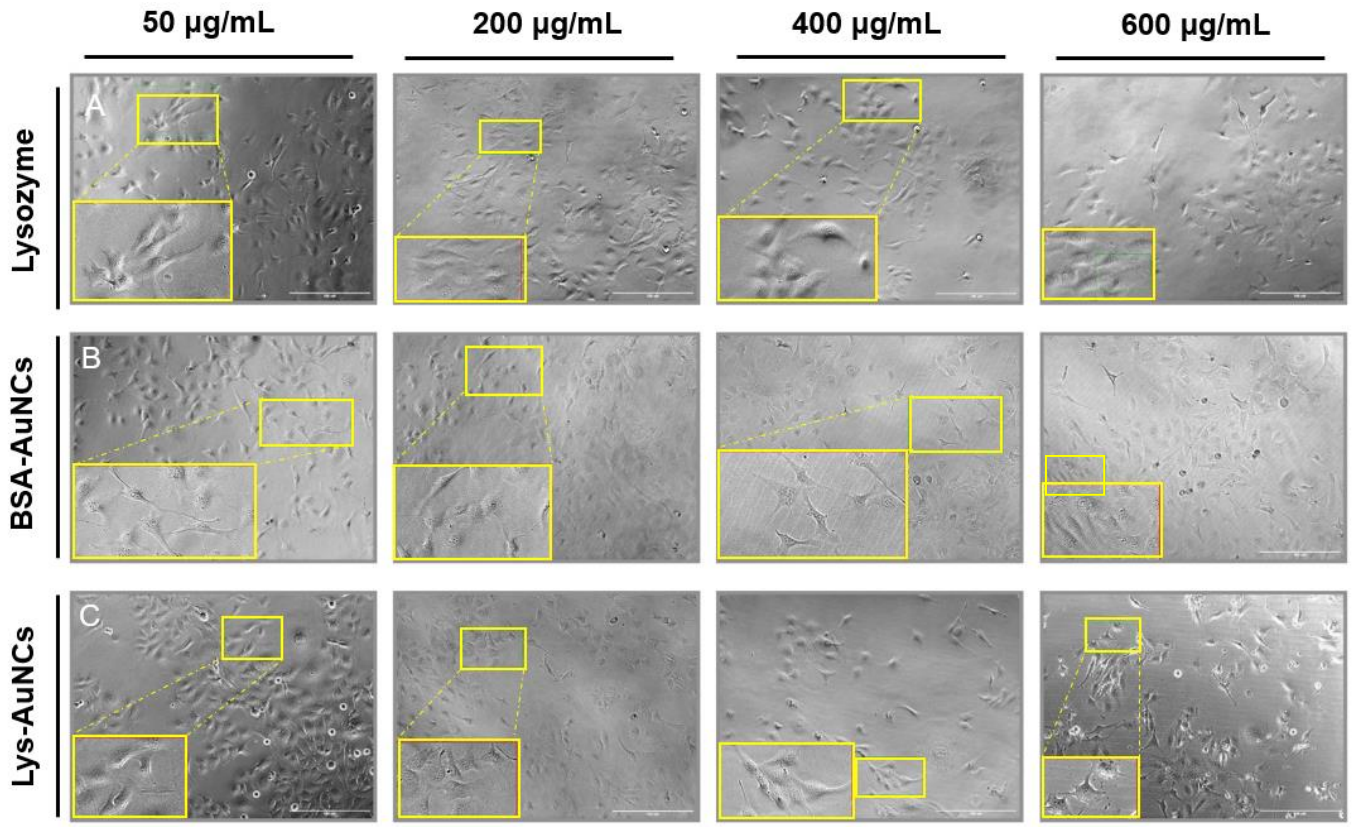

Figure 12. Morphology analysis of HMC3 cells treated with Lys-AuNCs. HMC3 cells were seeded at 8000 cells/mL and incubated (at 37ºC, 5% CO_2) for 24 hours then treated with lysozyme (**A**), BSA-AuNCs (**B**) and Lys-AuNCs (**C**) at concentrations of 50-600 µg/mL to incubate for a further 24 hours. Phase images were taken using an EVOS FL AUTO microscope at x 20 magnification (n=3). Scale bar 400 µM.

3.6 IBA1 staining shows activated HMC3 cells induced by Lys-AuNCs

To further confirm the morphological changes of HMC3 cells after treatment with Lys-AuNCs we next performed ICC-F staining with IBA1 a microglial-specific marker (Fig 13). Optimisation studies were completed prior to ICC-F staining to assess the optimal dilution for the IBA1 antibody (Table 2). Cells were stained with varying dilutions of the antibody ranging from 1:100, 1:250 and 1:1000. It was shown that a 1:100 dilution with final concentration of 10 µg/mL of the IBA1 was adequate for staining.

In general, varying phenotypes of microglia are identified through their morphology with 'resting' cells possessing a ramified morphology and 'activated' cells having formed an amoeboid phenotype. HMC3 cells without treatment (UT) showed expression of IBA-1 with

ramified morphology (Fig 13A). HMC3 cells were treated with LPS as a control for the microglia as this induces a pro-inflammatory response and these cells showed an increased level of IBA-1 expression with amoeboid cell morphology (Fig 13B). When treated with controls BSA-AuNCs and lysozyme, cells displayed higher IBA-1 expression than UT controls with a reduction in expression compared to LPS treated cells. HMC3 cells treated with Lys-AuNCs displayed increased IBA-1 expression suggesting an activated state (Fig 13E).

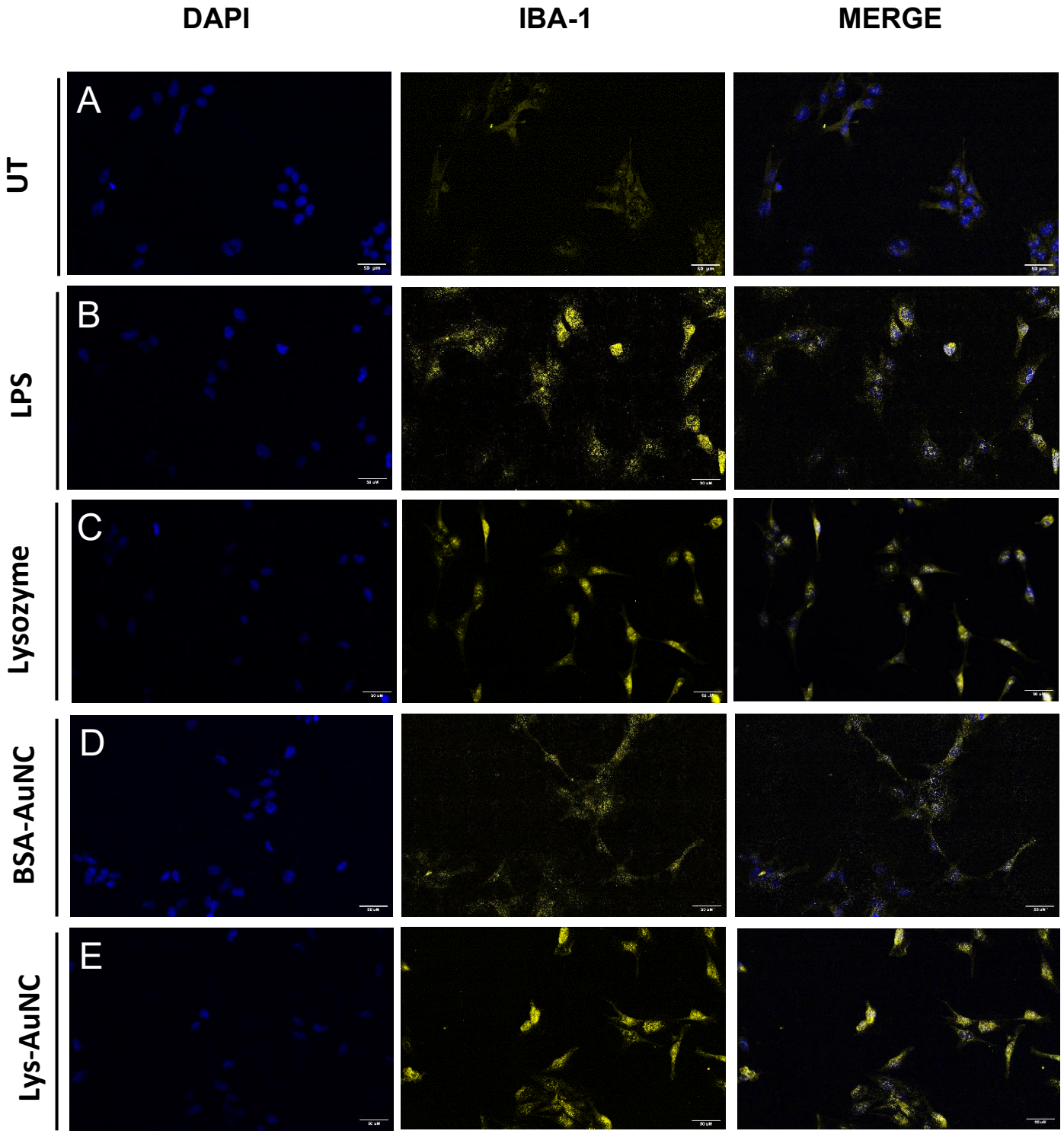

Figure 13. Expression of IBA1 by HMC3 cells after treatment with Lys-AuNCs, lysozyme and BSA-AuNCs. HMC3 cells were grown on glass coverslips for 24 hours, and treated with Lys-AuNCs, lysozyme and BSA-AuNCs at a concentration of 50 µg/mL. Cells were then stained with IBA-1 antibody (yellow fluorescence) and observed on an epifluorescent microscope with representative images acquired at x 20 magnification. Cells were counterstained with DAPI (blue fluorescence). Scale bar 50 µM.

IBA-1 expression was quantified by calculating the corrected total cell fluorescence (CTCF) as a measure of fluorescence intensity (FI) (Fig 14). Our data shows that cells left untreated displayed lower expression of IBA-1 with average FI measured per image of cell at 72172.3 which was increased to 138737.7 after treatment with 1 µg/mL of LPS (****p<0.0001). Cells treated with controls lysozyme and BSA-AuNCs also displayed a significantly lower expression of IBA-1 compared to LPS treated cells (103678.6, ****p<0.0001; 121227.2, ***p=0.001). Cells treated with Lys-AuNCs significantly increased IBA-1 expression compared to UT controls but did not show any marked change in IBA-1 expression compared to LPS treated cells which suggests a pro-inflammatory response. These findings suggest that the Lys-AuNCs induce an activated state in the HMC3 cells similar to that in the LPS treated cells.

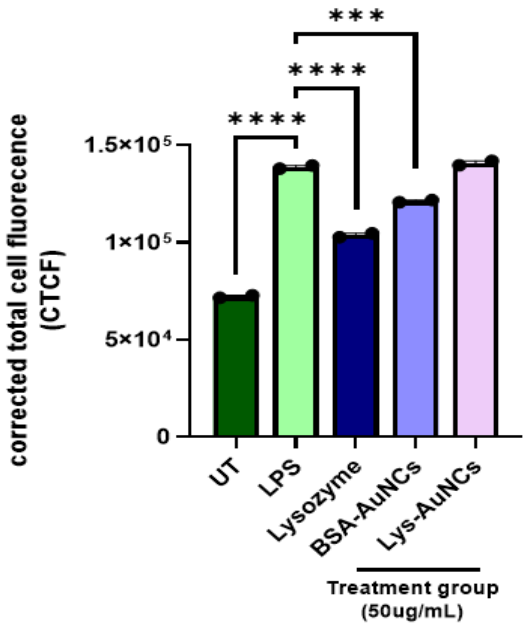

Figure 14. HMC3 cells treated with Lys-AuNCs show significantly higher expression of IBA1 compared to controls. HMC3 cells grown on glass coverslips were treated with Lys-AuNCs, lysozyme and BSA-AuNCs at a concentration of 50 µg/mL Images (as described

before) were processed using ImageJ software and IBA1 expression was quantified through calculating the corrected total cell fluorescence (CTCF) for each cell on 2 images per treatment group. HMC3 cells were treated with 1 µg/mL of LPS as a positive control for microglia. Data is presented as mean ± SEM and statistical significance determined using ONE-way ANOVA on GraphPad Prism 8.0, ***p=0.0001, ****p<0.0001. (n=2).

3.7 Production of immune cytokines and NO by HMC3 cells after treatment with Lys-AuNCs

To expand our understanding of how HMC3 cells respond to Lys-AuNC treatment we sought to assess their cytokine profiles after treatment with Lys-AuNCs. This will give an indication of the immune responses induced after treatment with the NCs. Based on our data from previous experiments we decided to use concentrations 10, 50, 200 and 400 µg/mL of Lys-AuNCs for ELISA assays as this concentration range induced minimal toxicity in HMC3 cells over 72 hours. After treatment, HMC3 cells were incubated for 24, 48 or 72 hours and centrifuged before collecting supernatant that was snap frozen on dry ice. Supernatant was then analysed by ELISA for concentrations of pro-inflammatory cytokines IL-6 a, TNFα, anti-inflammatory cytokine IL-10 was also assessed but the absence of cytokine production in samples and LPS positive controls indicates further optimisation is required. We also sought to assess any oxidative stress in HMC3 cells induced by Lys-AuNCs by measuring NO production in treated cells via a Griess-assay. The same supernatant used for ELISA assays at the same concentration range (10-400 µg/ mL) were used but no NO was detected in any samples including LPS controls implying an error with the cell line or the assay itself and further optimisation is required.

3.8 Effect of Lys-AuNCs on iNOS expression in HMC3s cells

Without the success of assays to assess the cytokine and NO profiles of HMC3 cells induced by Lys-AuNCs, we used immunostaining experiments to assess immune responses induced by Lys-AuNCs on HMC3 cells, staining was performed for inducible nitric oxide (iNOS) which is a pro-inflammatory mediator induced by microglia in response to pro-inflammatory stimuli. Cells were seeded at 10,000 cells/mL and grown on coverslips for 24 hours then treated with varying concentrations of Lys-AuNCs, lysozyme and BSA-AuNCs (5, 10, 50 and 200 µg/ mL) and incubated for a further 24 hours. HMC3 cells were also treated with 1 µg/mL of LPS to induce a pro-inflammatory response that generates activated microglia to express iNOS. iNOS

was identified by immunolabelling HMC3 cells with an anti-iNOS antibody (Fig 15). iNOS immunofluorescence was quantified by measuring the FI through calculating the mean CTCF of all cells per image using ImageJ software which was then averaged and plotted on a bar graph on GraphPad Prism 8.0 (Fig 16).

HMC3 cells left untreated show visibly low expression of iNOS as cells are typically in their 'resting' state (Fig 15D). HMC3 cell treated with LPS show higher iNOS expression due to induction of proinflammatory response (15E). HMC3s that were left untreated that should typically be in their 'resting' state had low expression of iNOS with FI measured at 39537.7 a.u. but after treatment with 10 µg/mL of Lys-AuNCs, HMC3s showed an increase in FI to 239442 a.u. (**p<0.01) (Fig 16B). Those treated with 5 µg/mL of lysozyme alone showed a slight increase in FI to 89075.4 a.u. (Fig 16A) and a further increase when treated with higher concentrations of 50 µg/mL to 162623 a.u. and 200 µg/mL to 174907 a.u. (*p<0.05,***p<0.001) (Fig 16C & D). HMC3 cells treated with 5 µg/mL of BSA-AuNCs showed an increase in FI to 137042 a.u. as well as 50 µg/mL (Fig 16A).

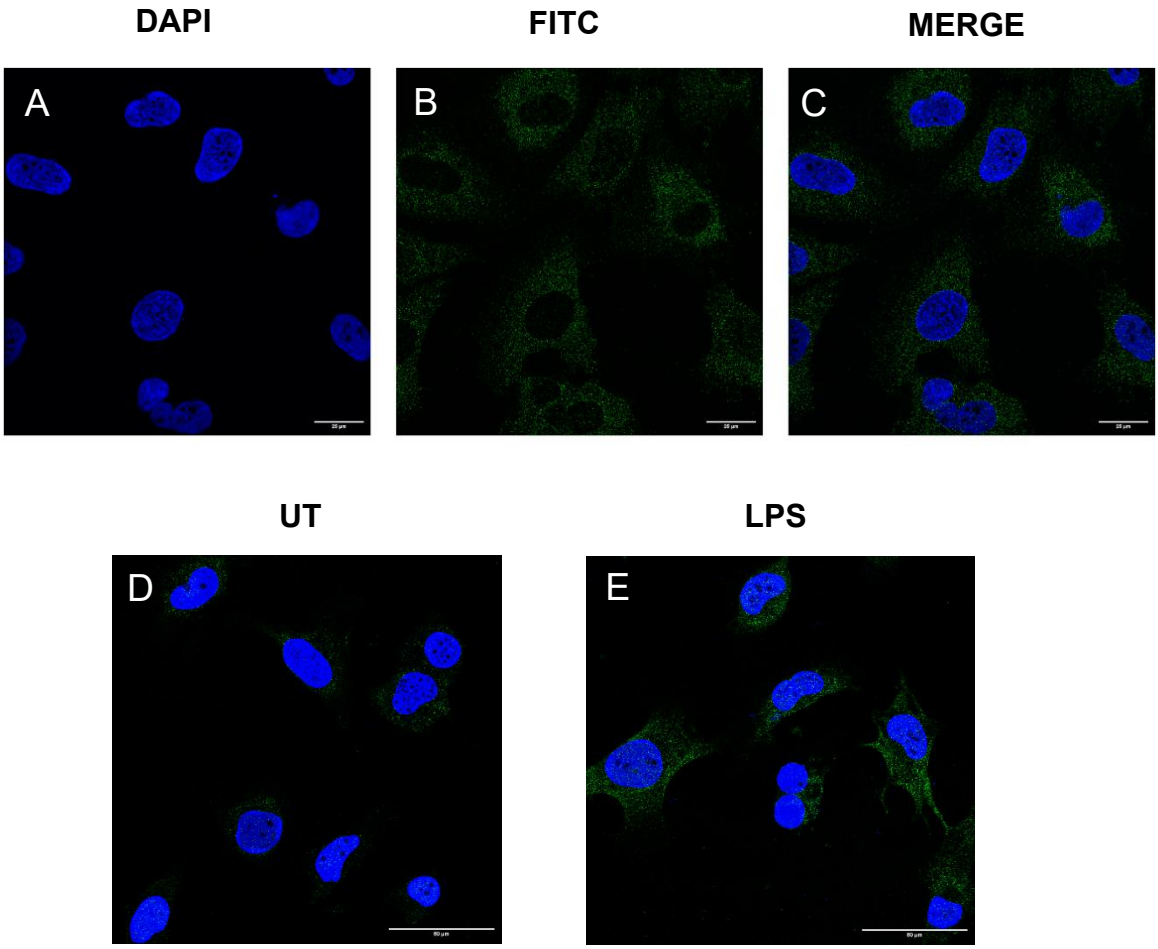

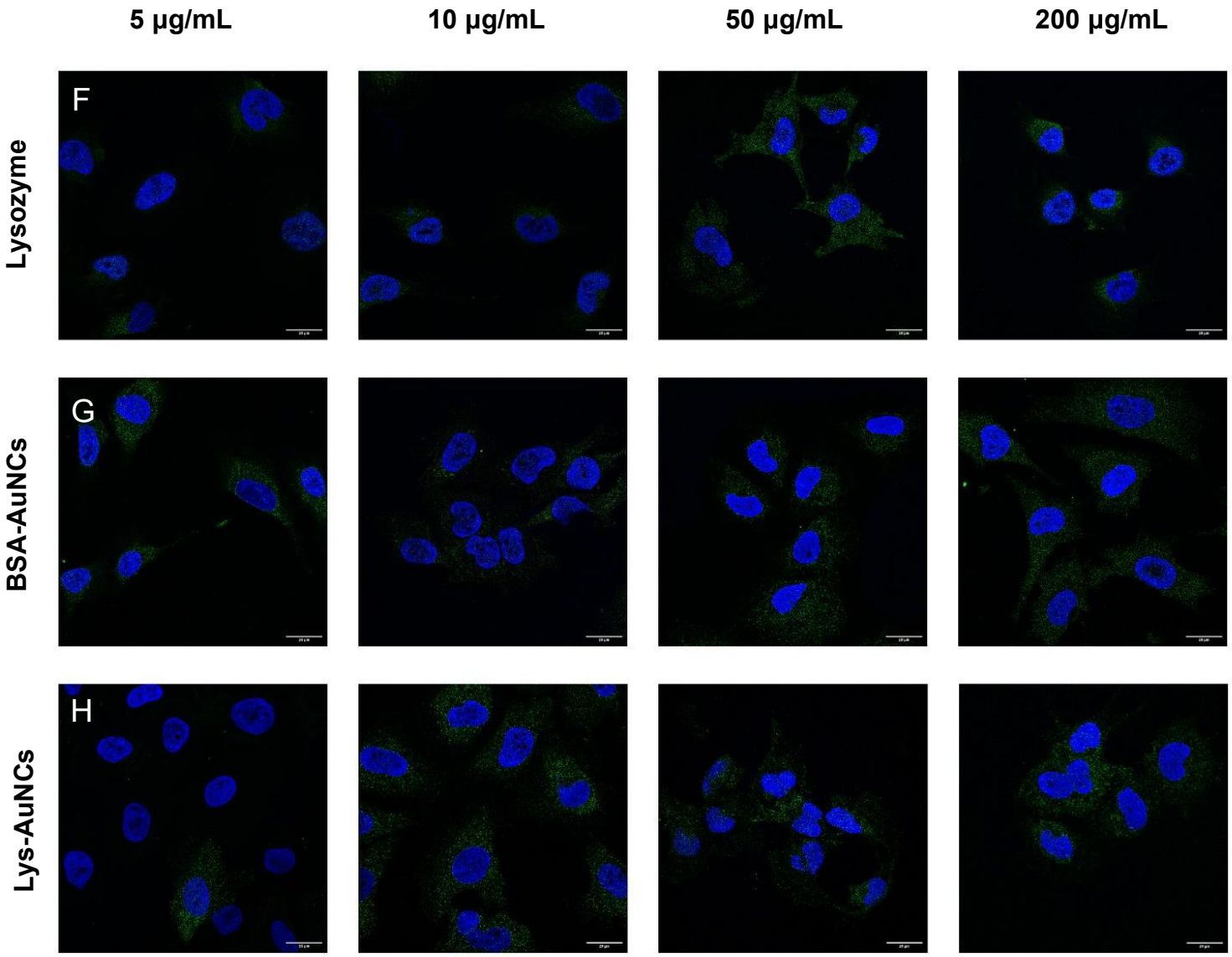

Figure 15. HMC3s show iNOS expression with pro-inflammatory stimulation and treatment with Lys-AuNCs. HMC3s were seeded at 10,000 cells/ mL on glass coverslips for 24 h (at 37ºC, 5% CO_2) then treated with Lys-AuNCs at concentrations of 5, 10, 50 and 200 µg/mL and lysozyme and BSA-AuNCs as controls and incubated as before for a further 24 hours. (**D, E**) Cells treated with 0 µg/ mL (UT) and 1 µg/ mL of LPS were used as controls. (**A-C**) Cells were labelled with iNOS (green fluorescence) and counterstained with DAPI (blue fluorescence). Images (1024 x 1024 pixels) were taken on a confocal Leica SP8 microscope at x 63 magnification and images merged using ImageJ software. Scale bar 25µM (**A-H**).

.

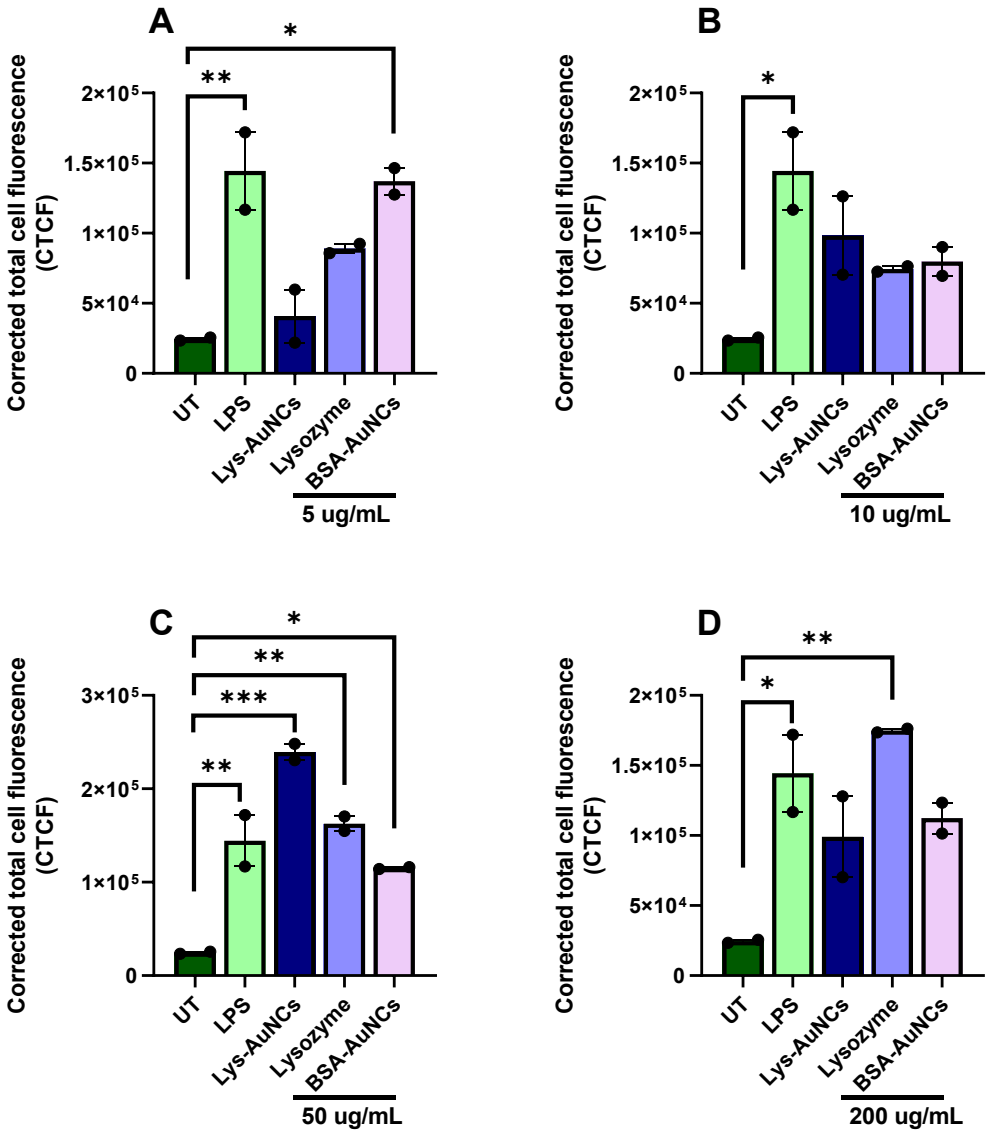

Figure 16. iNOS expression quantified in HMC3 cells treated with Lys-AuNCs via calculated total cell fluorescence (CTCF). HMC3s were seeded at 10,000 cells/ mL on glass coverslips for 24 h then treated with Lys-AuNCs as well as lysozyme and BSA-AuNCs as nanocluster controls at concentrations of 5 (A), 10 (B), 50 (C) and 200 µg/mL (D). Cells treated with 1 µg/mL of LPS and cells left untreated (UT) were included as negative and positive controls. After 24 hours of incubation, iNOS generation was quantified using ImageJ software and data expressed as means per duplicate ± SEM and statistical significance determined using ONE-way ANOVA on GraphPad Prism 8.0, *p<0.05, **p<0.01, ***p<0.001. (n=4).

To further assess the immune responses induced by Lys-AuNCs, HMC3 cells were stained with anti-inflammatory marker arg-1 which is a commonly used marker of alternatively activated microglia. HMC3 cells were seeded and treated as mentioned previously (Fig 16 & 17). Arg-1 was identified by immunolabelling HMC3 cells with an anti-arg-1 polyclonal (Fig 17A-E).

HMC3 cells left untreated show visibly high expression of arg-1 with cells typically in their 'resting' state (Fig 17A). HMC3 cell treated with LPS show lower arg-1 expression with the induction of pro-inflammatory response (17B).

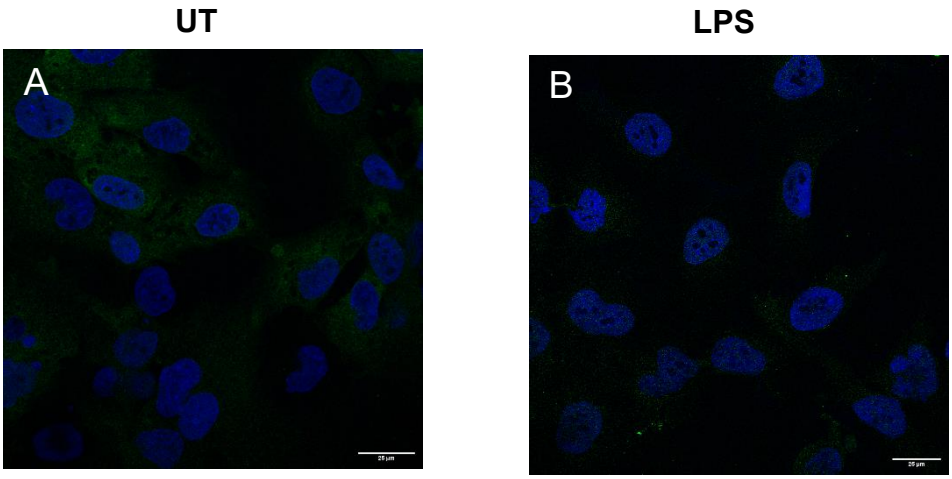

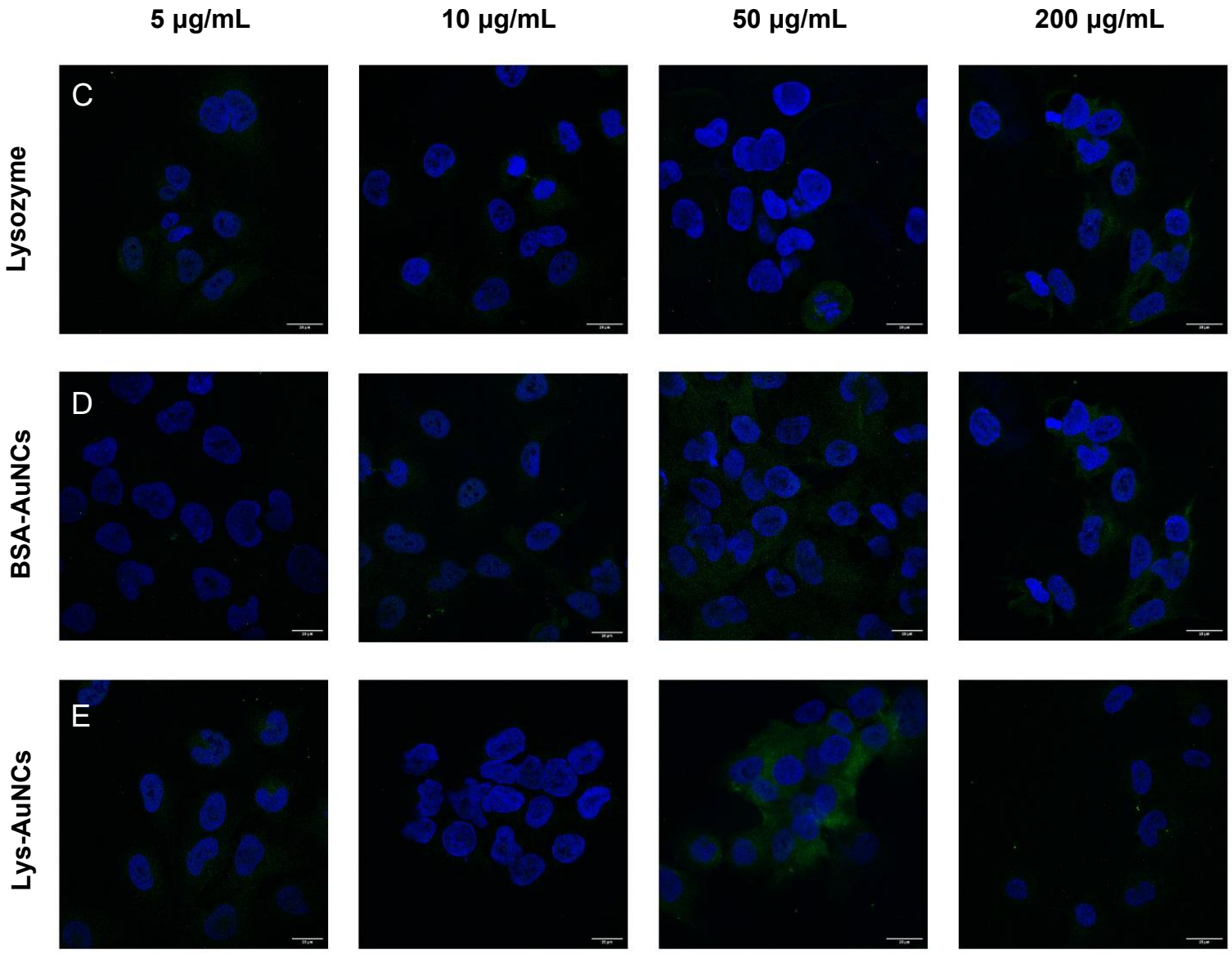

Figure 17. HMC3s left untreated show Arg-1 expression and treatment with lysozyme, BSA-AuNCs and Lys-AuNCs. HMC3s were seeded at 10,000 cells/ mL on glass coverslips for 24 h (at 37ºC, 5% CO_2) then treated with Lys-AuNCs at concentrations of 5, 10, 50 and 200 µg/mL and lysozyme and BSA-AuNCs alone incubated as before for a further 24 hours. Cells treated with 0 µg/ mL (UT) and 1 µg/ mL of LPS were used as controls. Cells were labelled with Arg-1 and counterstained with DAPI. Images (1024 x 1024 pixels) taken on a confocal Leica SP8 microscope at x 63 magnification and processed using ImageJ software. Scale bar 25 µM.

Arg-1 immunofluorescence was quantified through FI measured by calculating the mean CTCF of all cells per image taken for each treatment group using ImageJ software which was then averaged and plotted on a bar graph using GraphPad Prism 8.0 (Fig 18). Cells left untreated

showed high expression of arg-1 with average FI measured at 502457.5 a.u. but after treatment with 1μg/mL of LPS cells displayed a significant reduction in expression of arg-1 with FI measured at 107787 a.u. (****p<0.0001, Fig 18A-D). Similar to the effect of LPS treatment, cells treated with lysozyme alone showed a significant reduction in arg-1 expression across all concentrations (5-200 μg/mL) compared to UT controls (****p<0.0001, Fig 18A-D). Cells treated with BSA-AuNCs also showed a significant reduction in arg-1 expression across all concentrations (5-200μg/mL) compared to UT controls (****p<0.0001, Fig 18A-D). Cells treated with Lys-AuNCs showed a similar trend with lysozyme and BSA-AuNCs control groups with arg-1 expression significantly decreasing across all concentrations (****p<0.0001, Fig 18A-D).

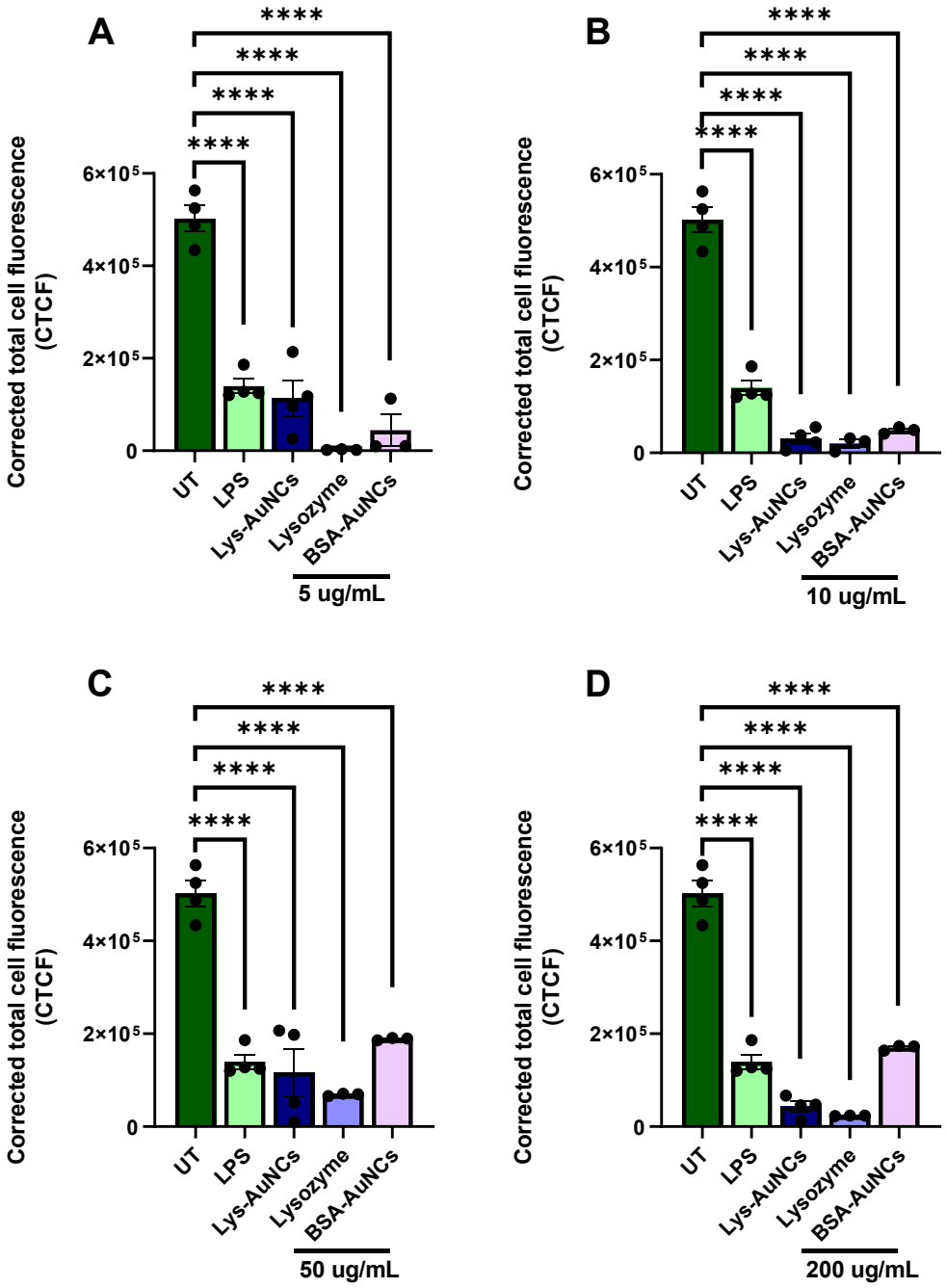

Figure 18. HMC3 cells show a significant decrease in Arg-1 expression compared to UT controls. HMC3s were seeded at 10,000 cells/ mL on glass coverslips for 24 h (at 37ºC, 5% CO_2) then treated with Lys-AuNCs as well as lysozyme and BSA-AuNCs as nanocluster controls at concentrations of 5 (A), 10 (B) 50 (C), 200 µg/mL (D). Cells treated with 1 µg/mL of LPS and cells left untreated (UT) were included as normalised controls and incubated as before for a further 24 hours. Arg-1 generation was quantified using ImageJ software and data

expressed as means ± SEM and statistical significance determined using ONE-way ANOVA on GraphPad Prism 8.0, ****p<0.001. (n=4).

4. Discussion

The aging population is an irreversible phenomenon with proportion aged 65 years and over expected to rise from 10% to 15% by 2050 (76). With our aging population, AD cases will continue to rise which only reiterates the need to further our understanding of the etiological mechanisms involved in AD (77). This could lead to advances in developing effective treatments to contain this public health crisis. Research provides sufficient evidence that glial cell mediated neuroinflammation plays a significant role in the pathogenesis of AD and therefore modulating the function of glial cells could potentially slow or prevent AD. Novel metal based nanoparticles have shown promise for effective disease modification with their ability to disrupt and inhibit Aβ plaque formation and neuroinflammation that drives AD. We therefore aimed to explore the possible influence of Lys-AuNCs on the microglial-mediated immune response and the resulting effects on AD pathology.

4.1 The characterisation of Lys-AuNCs

Successful synthesis of Lys-AuNCs ensuring optical and physiochemical properties remain intact throughout the synthesis process is the first essential step of this research project. In accordance with our experiments involving cell culture, we made relevant adjustments to the commonly used one-pot synthesis method for Lys-AuNCs by *Alkudaisi et al* (78). Lys-AuNCs were filtered after synthesis using a 0.22 μM filter to ensure the NC solutions were sterile preventing any potential contaminations with cell culture. During synthesis, the dialysis and filtration process of the Lys-AuNCs may alter their physicochemical properties which in turn would affect their final concentration. Given the novel nature of these nanoclusters any alterations to their structure could affect their physiochemical properties and hence their functionality (79). To ensure dialysis and filtration did not alter these properties we sought to confirm the Lys-AuNCs concentration throughout the synthesis process from dialysis and filtration, ensuring these concentrations are comparable to that of previous batches. To do this we generated a calibration curve relating the concentration of NCs pre-dialysis and after filtration. Concentrations of the nanoclusters showed consistency throughout synthesis and final concentration was comparable to previous batches confirming their optical and physiochemical properties remained intact through dialysis and filtration.

4.2 Lys-AuNCs do not induce toxicity in HMC3 cells

Despite extensive research, undesirable effects of nanoclusters are still not fully understood. We sought to assess any potential cell toxicity induced by Lys-AuNCs which is a good foundation for assessing Lys-AuNCs induced modulation of microglial function. Toxicity assays were performed over a 72 hour period and data showed no cell toxicity induced by Lys-AuNCs at concentrations of 50, 200 and 400 µg/mL but did at 600 µg/mL. Results can conclude that cells are able to tolerate high concentrations of Lys-AuNCs up to 48 hours. A similar effect was also observed in control groups with toxicity induced in cells at a concentration of 600 µg/ mL and those treated with BSA-AuNCs induced toxicity at concentrations 400 and 600 µg/mL. Given cell induced toxicity at high concentrations of Lys-AuNCs in future experiments we will be using lower concentrations of Lys-AuNCs with a maximum of 200 µg/mL which was the concentration used in a study by *Hillegass, J. M.* who also utilised an MTT assay to assess nanotoxicity in cells (80).

Since Lys-AuNCs show no toxicity at 600 µg/ mL after 48 hours this toxicity seen in lysozyme and BSA-AuNC treated cells at this time point could be due to protein induced affects. Decreased viability in BSA-AuNCs treated cells could be due to the gold and since BSA is a protein itself it could be exerting different effects to Lys-AuNCs. Since viability remains higher in Lys-AuNC treated cells, this could tell us that the lysozyme used as the stabilising agent with the gold nanocluster could be a beneficial combination. Our results show potential in that minimal toxicity is induced in microglial cells across a range of concentrations for an extended period of time, suggesting Lys-AuNCs are likely to be a safe agent used to treat cells and likely in vivo. These findings agree with a study done by *Ditta Ungor et al* who showed minimal influence of Lys-AuNCs on mammalian cell toxicity although undesirable cellular processes simulated by gold nanoclusters depends on the stabilising proteins (81).

It is important to consider the presented results from our studies are dependent on a measure of cell viability that relies on cellular metabolic activity and therefore does not directly measure cell-induced toxicity. The findings could be validated with an annexin V assay that directly measures cell cytotoxicity through indicating early-stage and late-stage apoptotic cells. This will distinguish cell death mechanisms occurring during potential cytotoxic responses and therefore precisely evaluate the contribution of apoptosis in the early stage of cell-mediated cytotoxicity induced by Lys-AuNCs.

4.3 Localisation of Lys-AuNCs in HMC3 cells

Assessing Lys-AuNCs localisation in relation to HMC3 cells could give us an indication whether the NCs are modulating responses intracellularly or extracellularly. Although Lys-AuNCs emit their own fluorescence in the infrared spectrum they are very small in size with a diameter of < 2nm. To aid visualisation of the small clusters we treated HMC3s with higher concentrations of Lys-AuNCs and captured Z-stack images on the confocal to produce 3D images of the cells to see their internal structures and components. This allows for in-depth imaging of Lys-AuNCs in HMC3 cells which has been done in a study by *Wei X et al* (82). Data showed intracellular localisation of Lys-AuNCs in HMC3 cells at 50 µg/ mL and 200 µg/mL. These results could be validated with a phalloidin stain to visualise the cytoskeleton of cells and confirm any potential extracellular localisation of Lys-AuNCs. A CellMask plasma membrane stain could also be used to visualise intracellular components and confirm intracellular localisation of Lys-AuNCs.

4.4 Activation of HMC3 cells by Lys-AuNCs

Since we have now confirmed no toxicity of Lys-AuNCs we sought to validate the HMC3 cell line used by examining cell morphology and their expression of microglial-specific marker IBA-1, expression of which correlates to microglial activation and inflammation (83, 84).

Morphological changes of microglial cells are indicative of their activation status and so we sought to assess any morphological changes of HMC3 cells induced by Lys-AuNCs at various concentrations between 50 to 600 µg/mL. Microglial cells exhibit different morphology depending on their activation state with typical 'resting' microglia displaying ramified morphology with small cell bodies, fine processes, and distal arborisation. Typical 'activated' microglia display intermediate morphology with enlarged cell bodies, retracted thick processes and decreased arborisation and phagocytic microglia display amoeboid morphology with enlarged cell bodies, loss of processes and lack of arborisation (85). Our data showed that HMC3 cells displayed no marked signs of activation although did generally show more activated morphology (with slightly enlarged cell bodies and thicker process) in Lys-AuNCs treated cells compared to control groups. Since there was no marked activated or phagocytic morphology our results could suggest that although the Lys-AuNCs are potentially inducing an activated state in the microglial cells, the cells are tolerating the treatment. We need to consider that these results are purely on observation, and they should be validated through

quantification of cell morphology. This could be done through Hematoxylin and Eosin (H & E) staining which allows for analysis of cell structure.

Lys-AuNCs treated HMC3s showed positive IBA1 staining and activated morphology, and although cells also displayed some amoeboid morphology it can be confirmed that Lys-AuNCs induce a state of activation in microglial cells. This was further confirmed by quantifying IBA-1 expression in the treated cells which confirmed that expression of IBA-1 induced by Lys-AuNCs was comparable to that induced by cells treated with LPS who should typically induce a pro-inflammatory response in HMC3 cells. Since IBA-1 is merely a marker of microglial activation nor pro- or anti-inflammatory based we cannot conclude that the Lys-AuNCs are steering towards a pro-inflammatory response but that they are inducing an activated state in microglial cells similar to that of LPS treated cells. This could be further investigated by quantifying IBA-1 expression in treatments co-stimulated with LPS as this would give us a more in-depth understanding of the immune responses being induced by the Lys-AuNCs. Studies have shown marker expression to differ in microglia with and without co-stimulation of pro-inflammatory mediators such as LPS and IFN-γ (86). CD68 and HLA-DR are other commonly microglial markers that could be used to further investigate microglial cell state. Both markers are upregulated by microglia in response to pro-inflammatory stimuli such as IFN-γ (87).

4.5 Immunogenicity of Lys-AuNCs on microglial cells

Since microglial induced immune responses have a key role in the development of AD it is essential to further understand the immunoregulatory effect of Lys-AuNCs on microglia. On expanding our assessment of immunogenicity of the Lys-AuNCs we sought to assess the pro- and anti-inflammatory profiles of microglia cells in response to treatment. This was attempted through quantitative ELISA assays of the supernatant collected from HMC3 cells treated with 10-400 μg/mL of Lys-AuNCs. We examined the levels of pro-inflammatory cytokines such as IL-6 and TNF-α and anti-inflammatory cytokines such as IL-10. On completion of these studies all results were below the negative threshold with no responses induced. Surprisingly we were also not able to detect any cytokine profiles after cells were treated with LPS, which has often been used as a positive control to induce activation and a pro-inflammatory response of microglial cells (88, 89, 90). The ELISA assays were performed in accordance with the correct protocols and performed to a good standard suggesting the assay did not work with our specific cells. This could be due to potential issues with the HMC3 cell line, which can be supported

by the lack of papers that have used this cell line. The LPS used might not be sufficient in inducing a pro-inflammatory response in the HMC3 cells alone and therefore future studies should involve a co-stimulation with other pro-inflammatory mediators such as IFN-γ to upregulate various activation markers of such as MHCII, CD68 and CD11b (91).

Neuroinflammation and oxidative stress (OS) in microglial cells contribute to the progression of AD leading to the activation of disease-associated microglia (DAM). DAM induce ROS via DAMPs by activation of NOX2 which is associated with DAMP signalling, inflammation, and amyloid plaque deposition in AD. To assess oxidative stress induced by Lys-AuNCs in microglia cells, nitric oxide (NO) release was measured via a Griess assay, however, results were negative. Our future experiments must confirm LPS validation and functionality with HMC3 cells with potential co-stimulation from another pro-inflammatory mediator.

4.6 Expression of iNOS and Arg-1 by HMC3 cells induced by Lys-AuNCs

On further investigation of oxidative stress, we sought to assess iNOS expression from cells as this is an important marker of microglial activation involved in the regulation of immune responses that can result in NO production and OS in AD (92). Cells treated with 5 μg/mL of lysozyme and BSA-AuNCs displayed a slight increase in iNOS expression and a further increase when treated with high concentrations of 50 and 200 μg/mL compared to UT controls. However, this dose dependant increase in iNOS expression was interrupted with no significant change in iNOS expression in cells treated with 10 μg/mL. In cells treated with Lys-AuNCs there was only a significantly higher expression of iNOS in cells treated with 50 μg/mL, since there is no direct comparison with control groups we cannot conclude if the Lys-AuNCs are leaning towards a favourable response. Our data could suggest that the combination of lysozyme and gold in the cluster could be beneficial as it is not inducing as much iNOS expression as the controls, however, this cannot be concluded as there is no direct data comparison with the control groups.

We sought to assess anti-inflammatory responses in the microglial cells to give us a better understanding of the immune responses induced by the Lys-AuNCs. This was done by assessing arg-1 expression which is an M2 or ‘alternatively activated’ marker of microglia that dampens inflammation through reduction of NO production from iNOS (93, 94). Cells treated with lysozyme and BSA-AuNCs showed a significant reduction in arg-1 expression across all concentrations compared to UT controls. Cells treated with LPS also showed a significantly

lower expression of arg-1 expression comparable to the treatments. Cells treated with Lys-AuNCs also showed a significant reduction in arg-1 expression across all concentrations. In order to confirm if this is the Lys-AuNCs leaning towards a pro-inflammatory response, our future studies should include cells pre-stimulated with LPS before treatment with Lys-AuNCs to assess if there are any changes in expression compared to treatments alone as this will give us a better understanding of the immune response being induced.

5. Conclusions and future directions

Our results have shown that we are able to successfully prepare Lys-AuNCs with consistent concentrations using an adapted synthesis method specific for cell culture whilst ensuring their physiochemical and optical properties remain intact throughout synthesis. Treatment with Lys-AuNCs can be seen to induce an activated state in microglial cells through changed cell morphology and positive IBA1 expression. Lys-AuNCs induce minimal cell toxicity in a range of concentrations less than 400µg/mL over a 72 hour period and display no marked iNOS expression in concentrations less than 50 µg/mL suggesting treatment with Lys-AuNCs may be preferred at low concentrations. Our data shows Lys-AuNCs are able to modulate microglial cell activation state and induce immune responses.

Our future studies should further investigate the toxicity of Lys-AuNCs through an annexin V assay or flow cytometry to give a direct measure of cell toxicity through indicating apoptotic properties and proportions of cells. The cytokine profiles of cells should be assessed by repeating ELISA experiments and/or PCR to assess inflammatory gene expression in treated cells. Our future studies should involve cells pre-treated with LPS or another pro-inflammatory mediator to compare this with unstimulated treatments to see if pro-inflammatory induction alters inflammatory expression in HMC3s induced by Lys-AuNCs, this will give an indication of what response is favoured. We should utilise the Lys-AuNCs emitting their own fluorescence by staining them in accompaniment with a microglia-specific marker or cytoskeleton stain to assess localisation of Lys-AuNCs in the cell and whether they are either extracellular and/or intracellular utilising z-stack imaging to assess specific location of Lys-AuNCs in or on the cells. Further analysis on oxidative stress induced by Lys-AuNCs should be assessed through repeating Griess assay to assess NO changes in response to Lys-AuNCs. Although microglia have such diverse functionality with multiple phenotypes that depend on activation state it would be interesting to look at other glial cells in communication with

microglia in the CNS, such as astrocytes and neurons and how Lys-AuNCs may affect their immune regulatory mechanisms that can lead to AD.

6. References

1. www.ons.gov.uk. (2022). Death Registration Summary statistics, England and Wales - OfficeforNationalStatistics.[online]Availableat:https://www.ons.gov.uk/peoplepopulationandcommunity/birthsdeathsandmarriages/deaths/articles/deathregistrationsummarystatisticsenglandandwales/2022.

2. Buffington AL, Lipski DM, Westfall E. Dementia: an evidence-based review of common presentations and family-based interventions. J Am Osteopath Assoc. 2013;113(10):768-75.

3. Gauthier. S. ea. World Alzheimer Report Life after diagnosis: Navigating treatment, care and support. Alzheimer's Disease International. 2022:25.

4. Gauthier S R-NP, Morais JA, & Webster C. . World Alzheimer Report 2021: Journey through the diagnosis of dementia. . Alzheimer’s Disease International. 2021:19.

5. Campion D, Dumanchin C, Hannequin D, Dubois B, Belliard S, Puel M, et al. Early-onset autosomal dominant Alzheimer disease: prevalence, genetic heterogeneity, and mutation spectrum. Am J Hum Genet. 1999;65(3):664-70.

6. Liu CC, Liu CC, Kanekiyo T, Xu H, Bu G. Apolipoprotein E and Alzheimer disease: risk, mechanisms and therapy. Nat Rev Neurol. 2013;9(2):106-18.

7. Wildsmith KR, Holley M, Savage JC, Skerrett R, Landreth GE. Evidence for impaired amyloid β clearance in Alzheimer's disease. Alzheimer's Research & Therapy. 2013;5(4):33.

8. Liu, C. C., Liu, C. C., Kanekiyo, T., Xu, H., & Bu, G. Apolipoprotein E and Alzheimer disease: risk, mechanisms and therapy. *Nature reviews. Neurology*. 2013;*9*(2), 106–118.

9. Hayashi H, et al. Apolipoprotein E-containing lipoproteins protect neurons from apoptosis via a signaling pathway involving low-density lipoprotein receptor-related protein-1. J Neurosci. 2007;27(8):1933–41.

10. Huang YA, et al. Differential Signaling Mediated by ApoE2, ApoE3, and ApoE4 in Human Neurons Parallels Alzheimer's Disease Risk. J Neurosci. 2019;39(37):7408–27.

11. Dubois, B., Hampel, H., Feldman, H. H., Scheltens, P., Aisen, P., Andrieu, S., Bakardjian, H., Benali, H., Bertram, L., Blennow, K., Broich, K., Cavedo, E., Crutch, S., Dartigues, J. F., Duyckaerts, C., Epelbaum, S., Frisoni, G. B., Gauthier, S., Genthon, R., Gouw, A. A., Proceedings of the Meeting of the International Working Group (IWG) and the American Alzheimer's Association on “The Preclinical State of AD”; July 23, 2015; Washington DC, USA. Preclinical Alzheimer's disease: Definition, natural history, and diagnostic criteria. *Alzheimer's & dementia : the journal of the Alzheimer's Association*. 2016;*12*(3), 292–323.

12. Bruni AC CM, Bernardi L. Genetics in degenerative dementia: current status and applicability. Alzheimer Dis. 2014;3:199-205.
13. Ritchie K, Ritchie CW, Yaffe K, Skoog I, Scarmeas N. Is late-onset Alzheimer's disease really a disease of midlife? Alzheimer's Dement (N Y). 2015;1(2):122-30.
14. Ju YE, Lucey BP, Holtzman DM. Sleep and Alzheimer disease pathology--a bidirectional relationship. Nat Rev Neurol. 2014;10(2):115-9.
15. Perry DC, Sturm VE, Peterson MJ, Pieper CF, Bullock T, Boeve BF, et al. Association of traumatic brain injury with subsequent neurological and psychiatric disease: a meta-analysis. J Neurosurg. 2016;124(2):511-26.
16. National Institute on Aging (2019). What Do We Know About Diet and Prevention of Alzheimer's Disease? *National Institutes of Health*. [online] 30 Nov. Available at: https://www.nia.nih.gov/health/what-do-we-know-about-diet-and-prevention-alzheimers-disease.
17. Rao YL, Ganaraja B, Murlimanju BV, Joy T, Krishnamurthy A, Agrawal A. Hippocampus and its involvement in Alzheimer's disease: a review. 3 Biotech. 2022;12(2):55.
18. Sabuncu, M. R., Desikan, R. S., Sepulcre, J., Yeo, B. T., Liu, H., Schmansky, N. J., Reuter, M., Weiner, M. W., Buckner, R. L., Sperling, R. A., Fischl, B., & Alzheimer's Disease Neuroimaging Initiative. The dynamics of cortical and hippocampal atrophy in Alzheimer disease. *Archives of neurology*. 2011;*68*(8), 1040–1048.
19. Hardy JA, and Higgins, G.A. Alzhiemer's disease: the amyloid cascade hypothesis. Science. 1992;256:184-5.
20. Colom-Cadena M, Spires-Jones T, Zetterberg H, Blennow K, Caggiano A, DeKosky ST, et al. The clinical promise of biomarkers of synapse damage or loss in Alzheimer's disease. Alzheimer's Research & Therapy. 2020;12(1):21.
21. Chow VW, Mattson MP, Wong PC, Gleichmann M. An overview of APP processing enzymes and products. Neuromolecular Med. 2010;12(1):1-12.
22. Denver P, English A, McClean PL. Inflammation, insulin signaling and cognitive function in aged APP/PS1 mice. *Brain Behav Immun.* 2018;70:423–434.
23. Villeneuve S, Rabinovici GD, Cohn-Sheehy BI, Madison C, Ayakta N, Ghosh PM, et al. Existing Pittsburgh Compound-B positron emission tomography thresholds are too high: statistical and pathological evaluation. Brain. 2015;138(Pt 7):2020-33.
24. Thal DR, Rüb U, Orantes M, Braak H. Phases of A beta-deposition in the human brain and its relevance for the development of AD. Neurology. 2002;58(12):1791-800.

25. LaFerla FM, Oddo S. Alzheimer's disease: A beta, tau and synaptic dysfunction. *Trends Mol Med.* 2005;11:170–176.

26. Zhao J, Liu X, Xia W, Zhang Y, Wang C. Targeting Amyloidogenic Processing of APP in Alzheimer's Disease. Frontiers in Molecular Neuroscience. 2020;13.

27. Price JL, Morris JC. Tangles and plaques in nondemented aging and "preclinical" Alzheimer's disease. *Ann Neurol.* 1999;45:358–368.

28. Kokjohn TA, Roher AE. Antibody responses, amyloid-beta peptide remnants and clinical effects of AN-1792 immunization in patients with AD in an interrupted trial. *CNS Neurol Disord Drug Targets.* 2009;8:88–97.

29. Holmes C, Boche D, Wilkinson D, Yadegarfar G, Hopkins V, Bayer A, Jones RW, Bullock R, Love S, Neal JW, Zotova E, Nicoll JA. Long-term effects of Abeta42 immunisation in Alzheimer's disease: follow-up of a randomised, placebo-controlled phase I trial. *Lancet.* 2008;372:216–223.

30. Gulisano W, Maugeri D, Baltrons MA, Fa M, Amato A, Palmeri A, D'Adamio L, Grassi C, Devanand DP, Honig LS, Puzzo D, Arancio O. Role of amyloid-beta and tau proteins in Alzheimer's disease: confuting the amyloid cascade. *J Alzheimers Dis.* 2018;64:S611–s631.

31. Garcia de Ancos J, Correas I, Avila J. Differences in microtubule binding and self-association abilities of bovine brain tau isoforms. J Biol Chem. 1993;268:7976-7982.

32. Ebneth A, Godemann R, Stamer K, Illenberger S, Trinczek B, Mandelkow E. Overexpression of tau protein inhibits kinesin-dependent trafficking of vesicles, mitochondria, and endoplasmic reticulum: implications for Alzheimer's disease. J Cell Biol. 1998;143(3):777-94.

33. Takashima A. Mechanism of neurodegeneration through tau and therapy for Alzheimer's disease. J Sport Health Sci. 2016;5(4):391-2.

34. Gong CX, Iqbal K. Hyperphosphorylation of microtubule-associated protein tau: a promising therapeutic target for Alzheimer disease. Curr Med Chem. 2008;15(23):2321-8.

35. Saha, P., & Sen, N. Tauopathy: A common mechanism for neurodegeneration and brain aging. *Mechanisms of ageing and development*. 2019; *178*, 72–79.

36. Busche MA, Hyman BT. Synergy between amyloid-β and tau in Alzheimer's disease. Nat Neurosci. 2020;23(10):1183-93.

37. Jessen K.R. Glial cells. Int. J. Biochem. Cell Biol. 2004;36:1861–1867.

38. Griffin WS . Inflammation and neurodegenerative diseases. *Am J Clin Nutr*. 2006; 83: 470S–474S.

39. Burda JE, Sofroniew MV. Reactive gliosis and the multicellular response to CNS damage and disease. Neuron. 2014;81(2):229-48.

40. Cai, Y., Liu, J., Wang, B., Sun, M., & Yang, H. Microglia in the Neuroinflammatory Pathogenesis of Alzheimer's Disease and Related Therapeutic Targets. Frontiers in immunology. 2022;13, 856376.

41. Gao, C., Jiang, J., Tan, Y. *et al.* Microglia in neurodegenerative diseases: mechanism and potential therapeutic targets. *Sig Transduct Target Ther. 2023;***8**, 359.

42. Blinzinger K, Kreutzberg G. Displacement of synaptic terminals from regenerating motoneurons by microglial cells. *Z fur Zellforschung und Mikroskopische Anatomie*. 1968;85:145–57.

43. Tremblay ME, Zettel ML, Ison JR, Allen PD, Majewska AK. Effects of aging and sensory loss on glial cells in mouse visual and auditory cortices. *Glia*. 2012;60:541–58.

44. Wake H, Moorhouse AJ, Jinno S, Kohsaka S, Nabekura J. Resting microglia directly monitor the functional state of synapses *In vivo* and determine the fate of ischemic terminals. *J Neurosci*. 2009;29:3974–80.

45. Spangenberg EE, Green KN. Inflammation in Alzheimer's disease: Lessons learned from microglia-depletion models. Brain Behav Immun. 2017;61:1-11.

46. Liddelow SA, Guttenplan KA, Clarke LE, Bennett FC, Bohlen CJ, Schirmer L, et al. Neurotoxic reactive astrocytes are induced by activated microglia. Nature. 2017;541(7638):481-7.

47. Brown GC, Neher JJ. Inflammatory Neurodegeneration and Mechanisms of Microglial Killing of Neurons. Molecular Neurobiology. 2010;41(2):242-7.

48. Nathan, C., Calingasan, N., Nezezon, J., Ding, A., Lucia, M. S., La Perle, K., Fuortes, M., Lin, M., Ehrt, S., Kwon, N. S., Chen, J., Vodovotz, Y., Kipiani, K., & Beal, M. F. Protection from Alzheimer's-like disease in the mouse by genetic ablation of inducible nitric oxide synthase. *The Journal of experimental medicine*. 2005;*202*(9), 1163–1169.

49. Cherry, J. D., Olschowka, J. A., & O'Banion, M. K. Arginase 1+ microglia reduce Aβ plaque deposition during IL-1β-dependent neuroinflammation. *Journal of neuroinflammation*. 2015;*12*, 203.

50. Hendrickx DAE, van Eden CG, Schuurman KG, Hamann J, Huitinga I. Staining of HLA-DR, Iba1 and CD68 in human microglia reveals partially overlapping expression depending on cellular morphology and pathology. J Neuroimmunol. 2017;309:12-22.

51. Jonsson T, Stefansson H, Steinberg S, Jonsdottir I, Jonsson PV, Snaedal J, et al. Variant of TREM2 associated with the risk of Alzheimer's disease. N Engl J Med. 2013;368(2):107.

52. Zheng H, Jia L, Liu CC, Rong Z, Zhong L, Yang L, et al. TREM2 Promotes Microglial Survival by Activating Wnt/β-Catenin Pathway. J Neurosci. 2017;37(7):1772-84.

53. Gratuze M., Leyns C.E.G., Holtzman D.M. New insights into the role of TREM2 in Alzheimer's disease. *Mol. Neurodegener.* 2018;13:66.

54. Hansen, D. V., Hanson, J. E., & Sheng, M. Microglia in Alzheimer's disease. *The Journal of cell biology*. 2018;*217*(2), 459–472.

55. Randall J. Bateman MD, Chengjie Xiong, Ph.D., Tammie L.S. Benzinger, M.D., Ph.D., Anne M. Fagan, Ph.D., et al. Clinical and Biomarker Changes in Dominantly Inherited Alzheimer's Disease. N Engl J Med. 2012;367:795-804.

56. Sperling R. A., Aisen P. S., Beckett L. A., Bennett D. A., Craft S., Fagan A. M., et al... Toward defining the preclinical stages of Alzheimer's disease: recommendations from the National Institute on Aging-Alzheimer's Association workgroups on diagnostic guidelines for Alzheimer's disease. *Alzheimer's Dement.* 2011;7, 280–292.

57. Aisen, P. S., Cummings, J., Jack, C. R., Jr, Morris, J. C., Sperling, R., Frölich, L., Jones, R. W., Dowsett, S. A., Matthews, B. R., Raskin, J., Scheltens, P., & Dubois, B. (2017). On the path to: understanding the Alzheimer's disease continuum. *Alzheimer's research & therapy*. 2025;*9*(1), 60.

58. McDade E, Cummings JL, Dhadda S, Swanson CJ, Reyderman L, Kanekiyo M, Koyama A, Irizarry M, Kramer LD, Bateman RJ. Lecanemab in patients with early Alzheimer's disease: detailed results on biomarker, cognitive, and clinical effects from the randomized and open-label extension of the phase 2 proof-of-concept study. Alzheimers Res Ther. 2022;14(1):191.

59. NICE (2018). *Recommendations | Dementia: Assessment, management and support for people living with dementia and their carers | Guidance | NICE*. [online] Nice.org.uk. Available at: https://www.nice.org.uk/guidance/NG97/chapter/Recommendations#pharmacological-management-of-alzheimers-disease.

60. Lilly (2023). *Lilly's Donanemab Significantly Slowed Cognitive and Functional Decline in Phase 3 Study of Early Alzheimer's Disease*. [online] Available at: https://investor.lilly.com/node/48836/pdf.

61. NICE (2011). *1 Recommendations | Donepezil, galantamine, rivastigmine and memantine for the treatment of Alzheimer's disease | Guidance | NICE*. [online] Nice.org.uk. Available at: https://www.nice.org.uk/guidance/ta217/chapter/1-Recommendations

62. Liu, J., Chang, L., Song, Y., Li, H., & Wu, Y. The Role of NMDA Receptors in Alzheimer's Disease. *Frontiers in neuroscience*. 2019;*13*, 43.

63. Jeevanandam J, Barhoum A, Chan YS, Dufresne A, Danquah MK. Review on nanoparticles and nanostructured materials: history, sources, toxicity and regulations. Beilstein J Nanotechnol. 2018;9:1050.

64. Moyano, D.F., Liu, Y., Ayaz, F., Hou, S., Puangploy, P., Duncan, B., Osborne, B.A. and Rotello, V.M. Immunomodulatory Effects of Coated Gold Nanoparticles in LPS-Stimulated In Vitro and In Vivo Murine Model Systems. *Chem*, [online]. 2016;1(2), pp.320–327.

65. Liao, Y.-H., Chang, Y.-J., Yoshiike, Y., Chang, Y.-C. and Chen, Y.-R. Negatively Charged Gold Nanoparticles Inhibit Alzheimer's Amyloid-β Fibrillization, Induce Fibril Dissociation, and Mitigate Neurotoxicity. *Small*. 2012;8(23), pp.3631–3639.

66. Pinheiro RGR, Coutinho AJ, Pinheiro M, Neves AR. Nanoparticles for Targeted Brain Drug Delivery: What Do We Know? Int J Mol Sci. 2021;22(21).

67. Hanada S, Fujioka K, Inoue Y, Kanaya F, Manome Y, Yamamoto K. Cell-based in vitro blood-brain barrier model can rapidly evaluate nanoparticles' brain permeability in association with particle size and surface modification. Int J Mol Sci. 2014;15(2):1812-25.

68. Jarmon, A. (2023). *What Is the Difference between Nanoparticles and Nanoclusters - Relationship between*. [online] relationshipbetween.com. Available at: https://relationshipbetween.com/what-is-the-difference-between-nanoparticles-and-nanoclusters/?expand_article=1 [Accessed 21 Nov. 2023].

69. Park, H.J., Shin, D.J. and Yu, J. Categorization of Quantum Dots, Clusters, Nanoclusters, and Nanodots. *Journal of Chemical Education*. 2021;98(3), pp.703–709.

70. Alkudaisi N, Russell, B.A., Birch, D.J.S. and Chen, Y. Lysozyme encapsulated gold nanoclusters for probing the early stage of lysozyme aggregation under acidic conditions. Journal of Photochemistry and Photobiology B: Biology. 2019;197.

71. Swaminathan R, Ravi VK, Kumar S, Kumar MV, Chandra N. Lysozyme: a model protein for amyloid research. Adv Protein Chem Struct Biol. 2011;84:63-111.

72. Luo, Y. H., Chang, L. W., & Lin, P. Metal-Based Nanoparticles and the Immune System: Activation, Inflammation, and Potential Applications. *BioMed research international*. 2015;143720.

73. Alkudaisi N, Russell BA, Birch DJS, Chen Y. Lysozyme encapsulated gold nanoclusters for probing the early stage of lysozyme aggregation under acidic conditions. Journal of Photochemistry and Photobiology B: Biology. 2019; 6.5, 139-141.

74. Liao Y-H, Chang Y-J, Yoshiike Y, Chang Y-C, Chen Y-R. Negatively Charged Gold Nanoparticles Inhibit Alzheimer's Amyloid-β Fibrillization, Induce Fibril Dissociation, and Mitigate Neurotoxicity. Small. 2012;8(23):3631-9.
75. Hou K, Zhao J, Wang H, Li B, Li K, Shi X, et al. Chiral gold nanoparticles enantioselectively rescue memory deficits in a mouse model of Alzheimer's disease. Nature Communications. 2020;11(1):4790.
76. Janabi, N., Peudenier, S., Héron, B., Ng, K. H., & Tardieu, M. Establishment of human microglial cell lines after transfection of primary cultures of embryonic microglial cells with the SV40 large T antigen. *Neuroscience letters*. 1995;*195*(2), 105–108.
77. Alvarez, P. (2023). Charted: The World's Aging Population from 1950 to 2100. [online] Visual Capitalist. Available at: https://www.visualcapitalist.com/cp/charted-the-worlds-aging-population-1950-to-2100/#:~:text=population%20across%20countries.-.
78. Alkudaisi N, Russell BA, Birch DJS, Chen Y. Lysozyme encapsulated gold nanoclusters for probing the early stage of lysozyme aggregation under acidic conditions. Journal of Photochemistry and Photobiology B: Biology. 2019;4.3, 4.3.1, 67-68.
79. Liu, X., Peng, F., Li, G., & Diao, K. Dynamic Metal Nanoclusters: A Review on Accurate Crystal Structures. *Molecules (Basel, Switzerland)*. 2023;*28*(14), 5306.
80. Hillegass, J. M., Shukla, A., Lathrop, S. A., MacPherson, M. B., Fukagawa, N. K., & Mossman, B. T. Assessing nanotoxicity in cells in vitro. *Wiley interdisciplinary reviews. Nanomedicine and nanobiotechnology*. 2010;*2*(3), 219–231.
81. Ungor D, Barbasz A, Czyżowska A, Csapó E, Oćwieja M. Cytotoxicity studies of protein-stabilized fluorescent gold nanoclusters on human lymphocytes. Colloids Surf B Biointerfaces. 2021;200:111593.
82. Wei, X., Li, H., Li, H., Zuo, Z., Song, F., Kang, X. and Zhu, M. Slice Visualization for Imaging Nanocluster Transformations. *Journal of the American Chemical Society*. 2023;145(25), pp.13750–13757.
83. Minett, T., Classey, J., Matthews, F. E., Fahrenhold, M., Taga, M., Brayne, C., Ince, P. G., Nicoll, J. A., Boche, D., & MRC CFAS. Microglial immunophenotype in dementia with Alzheimer's pathology. Journal of neuroinflammation. 2016;13(1), 135.
84. Ito D, Imai Y, Ohsawa K, Nakajima K, Fukuuchi Y, Kohsaka S. Microglia-specific localisation of a novel calcium binding protein, Iba1. Brain Res Mol Brain Res. 1998;57(1):1-9.

85. Lively, S., & Schlichter, L. C. Microglia Responses to Pro-inflammatory Stimuli (LPS, IFNγ+TNFα) and Reprogramming by Resolving Cytokines (IL-4, IL-10). *Frontiers in cellular neuroscience*. 2018;*12*, 215.
86. Edler MK, Mhatre-Winters I, Richardson JR. Microglia in Aging and Alzheimer's Disease: A Comparative Species Review. *Cells*. 2021; 10(5):1138.
87. Hendrickx, D.A.E., van Eden, C.G., Schuurman, K.G., Hamann, J. and Huitinga, I. Staining of HLA-DR, Iba1 and CD68 in human microglia reveals partially overlapping expression depending on cellular morphology and pathology. *Journal of Neuroimmunology*. 2017;309(0165-5728), pp.12–22.
88. Lu, Z., Liu, S., Lopes-Virella, M.F. and Wang, Z. LPS and palmitic acid Co-upregulate microglia activation and neuroinflammatory response. *Comprehensive Psychoneuroendocrinology*. 2021;6, p.100048.
89. Lively, S., & Schlichter, L. C. Microglia Responses to Pro-inflammatory Stimuli (LPS, IFNγ+TNFα) and Reprogramming by Resolving Cytokines (IL-4, IL-10). *Frontiers in cellular neuroscience*. 2018;*12*, 215.
90. Dello Russo, C., Cappoli, N., Coletta, I., Mezzogori, D., Paciello, F., Pozzoli, G., Navarra, P. and Battaglia, A. The human microglial HMC3 cell line: where do we stand? A systematic literature review. *Journal of Neuroinflammation*. 2018;15(1).
91. Li B, Bedard K, Sorce S, Hinz B, Dubois-Dauphin M, Krause KH. NOX4 expression in human microglia leads to constitutive generation of reactive oxygen species and to constitutive IL-6 expression. J Innate Immun. 2009;1:570–81.
92. Asiimwe, N., Yeo, S. G., Kim, M. S., Jung, J., & Jeong, N. Y. Nitric Oxide: Exploring the Contextual Link with Alzheimer's Disease. *Oxidative medicine and cellular longevity*. 2016;7205747.
93. Munder M, Eichmann K, Modolell M. Alternative metabolic states in murine macrophages reflected by the nitric oxide synthase/arginase balance: competitive regulation by CD4+ T cells correlates with Th1/Th2 phenotype. *J Immunol*. 1998;160:5347–54.
94. Rutschman R, Lang R, Hesse M, Ihle JN, Wynn TA, Murray PJ. Cutting edge: Stat6-dependent substrate depletion regulates nitric oxide production. *J Immunol*. 2001;166:2173–7.